7-21-2003

Cross-section measurements for the near ultra-violet absorption spectra of glyoxal at the 280 nanometer wavelength

Abigail Diaz
Florida International University

DOI: 10.25148/etd.FI14062268

FLORIDA INTERNATIONAL UNIVERSITY

Miami, Florida

CROSS-SECTION MEASUREMENTS FOR THE NEAR ULTRA-VIOLET ABSORPTION SPECTRA OF GLYOXAL AT THE 280 NANOMETER WAVELENGTH

A thesis submitted in partial fulfillment of the

requirements for the degree of

MASTER OF SCIENCE

in

CHEMISTRY

by

Abigail Diaz

2003

To: Dean Arthur W. Herriott
College of Arts and Sciences

This thesis, written by Abigail Diaz, and entitled Cross-Section Measurements for the Near Ultra-Violet Absorption Spectra of Glyoxal at the 280 Nanometer Wavelength, having been approved in respect to style and intellectual content, is referred to you for judgment.

We have read this thesis and recommend that it be approved.

David Chatfield

James M. Quirke

Jeffrey A. Joens, Major Professor

Date of Defense: July 21, 2003

The thesis of Abigail Diaz is approved.

Dean Arthur W. Herriott
College of Arts and Sciences

Dean Douglas Wartzok
University Graduate School

Florida International University, 2003

ACKNOWLEDGMENTS

I would like to thank Dr. Jeffrey Joens for his guidance and assistance during my research. I wish to also thank Dr. David Chatfield for his advice and aid in the development of my improved understanding of computational chemistry. A special token of gratitude goes to Dr. Palmer Graves, who supported me every step of the way.

Finally, I want to express my thanks to the chemistry faculty for their support and the part they played in my intellectual enrichment.

ABSTRACT OF THE THESIS

CROSS-SECTION MEASUREMENTS FOR THE NEAR ULTRA-VIOLET ABSORPTION SPECTRA OF GLYOXAL AT THE 280 NANOMETER WAVELENGTH

by

Abigail Diaz

Florida International University, 2003

Miami, Florida

Professor Jeffrey A. Joens, Major Professor

Glyoxal and other dicarbonyl compounds have been detected in tropospheric air in rural areas and polluted urban areas. Accurate absorption cross-sections for the near UV spectrum of glyoxal are important since the value of this chemical characteristic is necessary for calculating effective quantum yields and ultimately the rates and products of photolysis. In this study, comprehensive measurements were made for the 280 nm gas-phase absorption spectrum of glyoxal. In addition, molecular orbital calculations were carried out and the results used as a guide to identify the vibration responsible for the weak structure features of the continuous area of the glyoxal spectrum. That vibration was found to be an a_g CO stretch vibration mode of the glyoxal molecule.

TABLE OF CONTENTS

LIST OF TABLES

LIST OF FIGURES

Chapter I

Introduction

Dicarbonyl compounds such as glyoxal (CHOCHO) and methylglyoxal ($CH_3C(O)CHO$) have been measured in tropospheric air, in rural areas at small concentrations, and in polluted urban areas. Munger et al. [1995] report an average concentration of 44 ppt glyoxal in Central Virginia, and Lee et al. [1995] measured average glyoxal concentrations of 18-83 ppt and average methylglyoxal concentrations of 31-88 ppt at a rural site in Georgia. [Finlayson-Pitts and Pitts, 2000] Higher concentrations are found in urban air, for example, 0.78 ± 0.85 ppb glyoxal and 1.0 ± 0.6 ppb methylgloxal in the Los Angeles area. [Finlayson-Pitts and Pitts, 2000]

There is a growing interest as well as need to investigate the atmospheric loss processes of glyoxal and other dicarbonyl compounds in more detail. Accurate absorption cross-sections for the near UV spectra of these two molecules are important since the value of this chemical characteristic is necessary for calculating effective quantum yields and ultimately the rates and products of photolysis. Moreover, cross-section data are also of use for laboratory studies of glyoxal chemistry

Chapter I

Introduction

Dicarbonyl compounds such as glyoxal (CHOCHO) and methylglyoxal ($CH_3C(O)CHO$) have been measured in tropospheric air, in rural areas at small concentrations, and in polluted urban areas. Munger et al. [1995] report an average concentration of 44 ppt glyoxal in Central Virginia, and Lee et al. [1995] measured average glyoxal concentrations of 18-83 ppt and average methylglyoxal concentrations of 31-88 ppt at a rural site in Georgia. [Finlayson-Pitts and Pitts, 2000] Higher concentrations are found in urban air, for example, 0.78 ± 0.85 ppb glyoxal and 1.0 ± 0.6 ppb methylgloxal in the Los Angeles area. [Finlayson-Pitts and Pitts, 2000]

There is a growing interest as well as need to investigate the atmospheric loss processes of glyoxal and other dicarbonyl compounds in more detail. Accurate absorption cross-sections for the near UV spectra of these two molecules are important since the value of this chemical characteristic is necessary for calculating effective quantum yields and ultimately the rates and products of photolysis. Moreover, cross-section data are also of use for laboratory studies of glyoxal chemistry

where glyoxal concentration is determined by absorption spectroscopy.

There are presently several inconsistencies in the published measurements of absorption cross-sections of glyoxal, as is discussed below.

In the present work, comprehensive measurements have been made for the gas phase absorption spectrum of glyoxal. The results from these measurements can be used to estimate the lifetime of glyoxal with respect to photodissociation for a representative set of tropospheric conditions.

In addition, molecular orbital calculations were also carried out and the results compared to what was observed experimentally and to previous results. The molecular orbital calculations were also used as a guide to identify the vibration responsible for the weak structured features of the continuous area of the spectrum.

Properties of glyoxal

Glyoxal is an organic molecule with a molecular formula of $C_2H_2O_2$. (See Figure 1.1) Glyoxal is a powerfully reducing and reactive solid (yellow prisms or irregular pieces turning white on cooling) with a melting point of 15°C and of high vapor pressure and low boiling point of 50°C. [Bretherick, 1985] Mixtures of glyoxal with air may explode, and contact with water causes violent

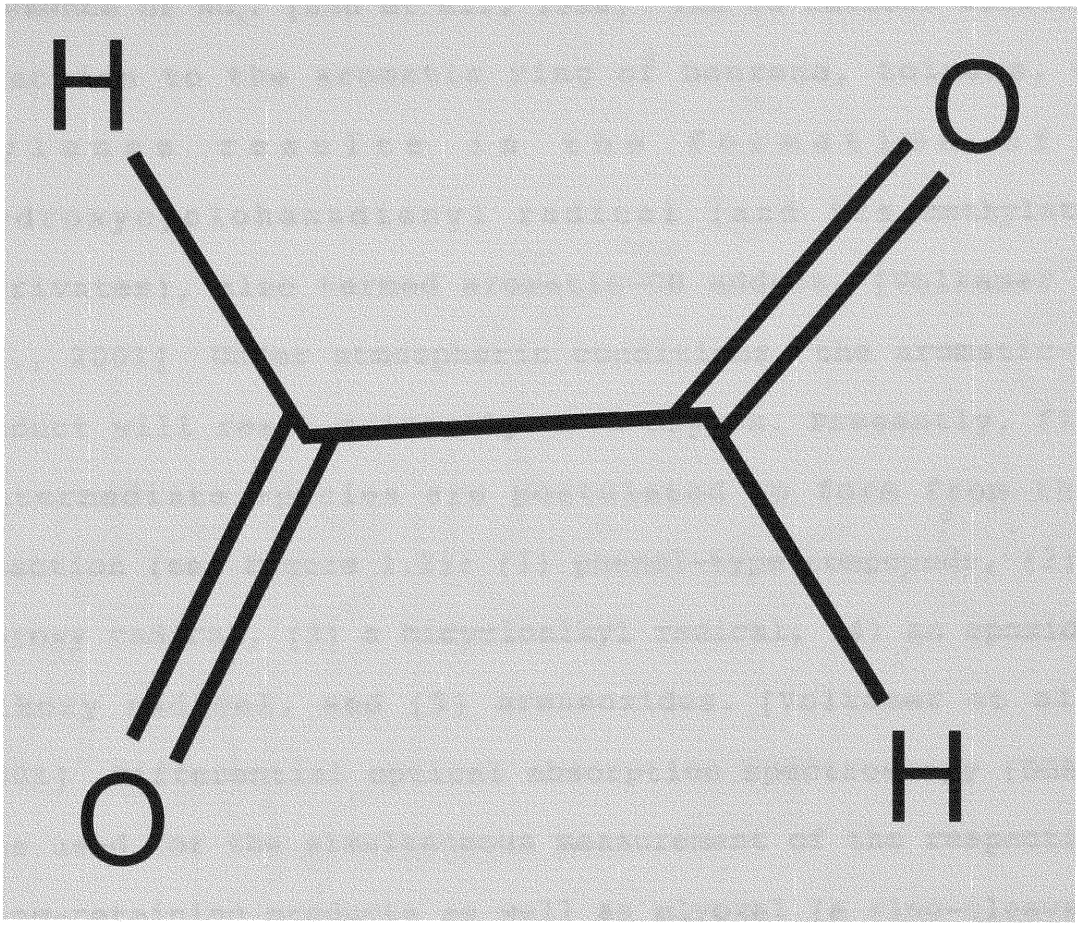

Figure 1.1. Drawing of trans-glyoxal molecule.

polymerization. [Bretherick, 1985] Like formaldehyde, pure glyoxal may polymerize exothermally and ignite in storage. When heated to decomposition it emits acrid smoke and irritating vapors. [Lewis, 1997]

Atmospheric chemistry of glyoxal

Glyoxal is an important ring-cleavage product in the air photo-oxidation of some aromatic hydrocarbons in the

presence of NO_x. [Zhu et al., 1996] The OH radical addition reaction to the aromatic ring of benzene, toluene, or xylenes results in the formation of a hydroxycyclohexadienyl radical (and its methylated derivates), also termed aromatic-OH adduct. [Volkamer et al., 2001] Under atmospheric conditions, the aromatic-OH adduct will react primarily with oxygen. Presently, five intermediate species are postulated to form from this reaction (see Figure 1.2): (1) phenol-type compounds, (2) a peroxy radical, (3) a bicycloalkyl radical, (4) an epoxide-alkoxy radical, and (5) areneoxides. [Volkamer et al., 2001] Differential optical absorption spectroscopy (DOAS) was used for the simultaneous measurement of the respective ring-retaining products as well as glyoxal (a ring-cleavage product) in a series of experiments at the EUPHORE, large outdoor simulation chamber in Valencia, Spain. [Volkamer et al., 2001] The ring-retaining products and glyoxal were identified as primary products. According to this study, the yield of glyoxal was determined to be 35% ± 10% from benzene and about 5% higher from toluene and *p*-xylene. [Volkamer et al., 2001] They noted that the error of the absolute glyoxal yield determined in their study is dominated by the uncertainty of the UV absorption cross-sections of glyoxal and that an improved determination is

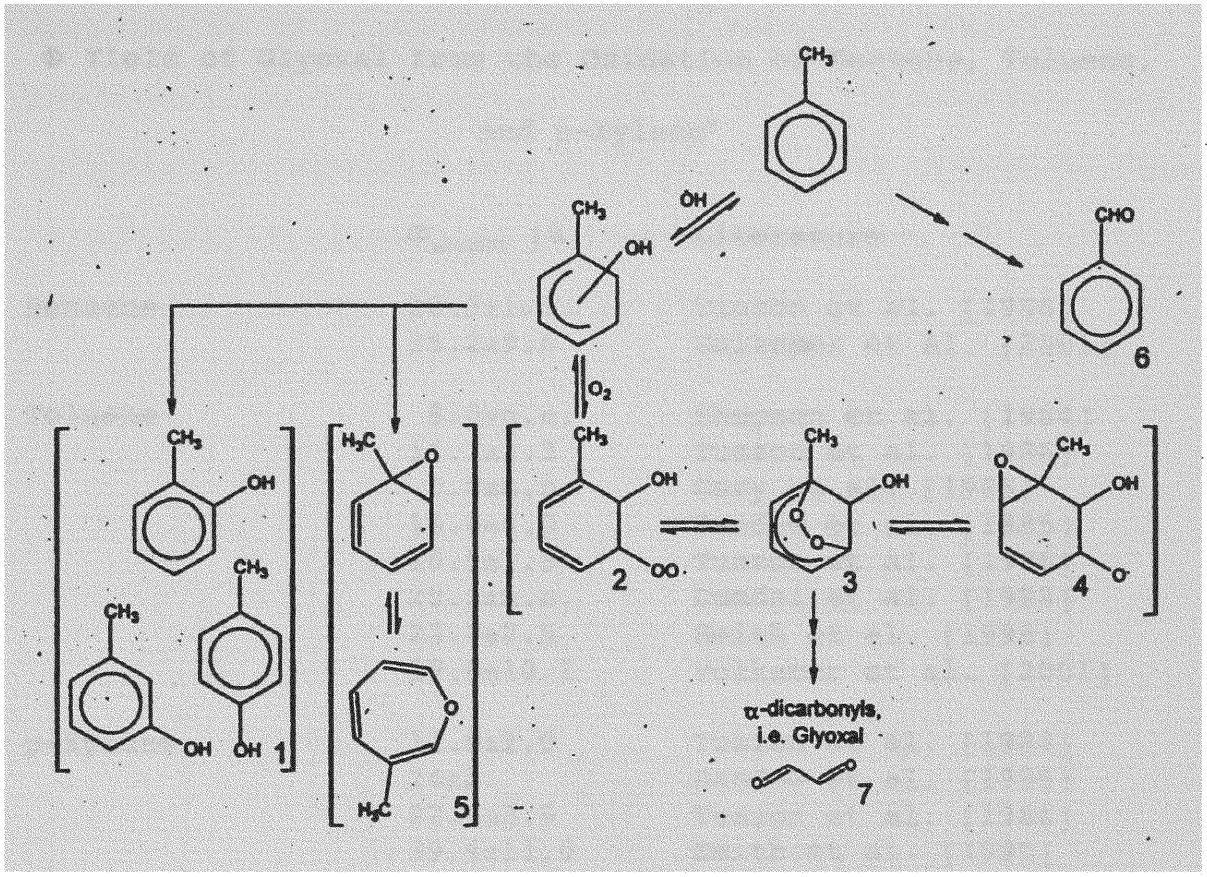

Figure 1.2. Initial steps of the OH radical initiated oxidation of toluene. Analogous intermediates are proposed for benzene and *p*-xylene. [Volkamer et al., 2001]

desirable. A comparison of glyoxal yields for OH and the aforementioned aromatic compounds of previous years can be seen in Table 1.1. [Volkamer et al., 2001]

The additional yet negligible contribution of pathways forming glyoxal through the OH reaction of stable intermediate compounds is due to the dominant photolysis of

Table 1.1

Φ Yield of Glyoxal from the Oxidation of Benzene, Toluene, and p-Xylene[a]

	$\Phi_{product}$ [%]	Literature
Benzene	20.7±1.9	Tuazon et al. [1986]
	35.2±9.6	Volkamer et al. [2001]
Toluene	8.0±n.n.	Shepson et al. [1984]
	11.1±1.3	Tuazon et al. [1986]
	9.8±n.n.	Gery et al. [1985]
	15.0±4.0	Bandow et al. [1985]
	10.5±1.9	Tuazon et al. [1986]
	20.3±n.n.	Dumdei et al. [1988]
	23.8±2.5	Smith et al. [1998]
	39.0±10.2	Volkamer et al. [2001]
p-Xylene	12.0±2.0	Tuazon et al. [1984]
	24±2	Bandow et al. [1985]
	22.5±3.9	Tuazon et al. [1986]
	39.4±11.0	Smith et al. [1999]
	40.4±10.6	Volkamer et al. [2001]

a) Volkamer et al. [2001]

potential precursors for secondary glyoxal, i.e. unsaturated 1,4-dicarbonyl-type products. Formation of butenedial from toluene and *o*-xylene, 4-oxo-2-pentenol from toluene and *o*- and *m*-xylene, and 3-hexene-2,5-dione from *p*-xylene and 1,2,4-trimethylbenzene have all been experimentally observed and are postulated as ring cleavage

carbonyl products during the OH-initiated atmospheric degradation of those aromatic hydrocarbons. [Lui et al., 1999 and Smith et al., 1999] In principle, any intermediate compound seen in Figure 1.3 may result in the formation of glyoxal as primary, secondary, or higher-generation product. [Volkamer et al., 2001]

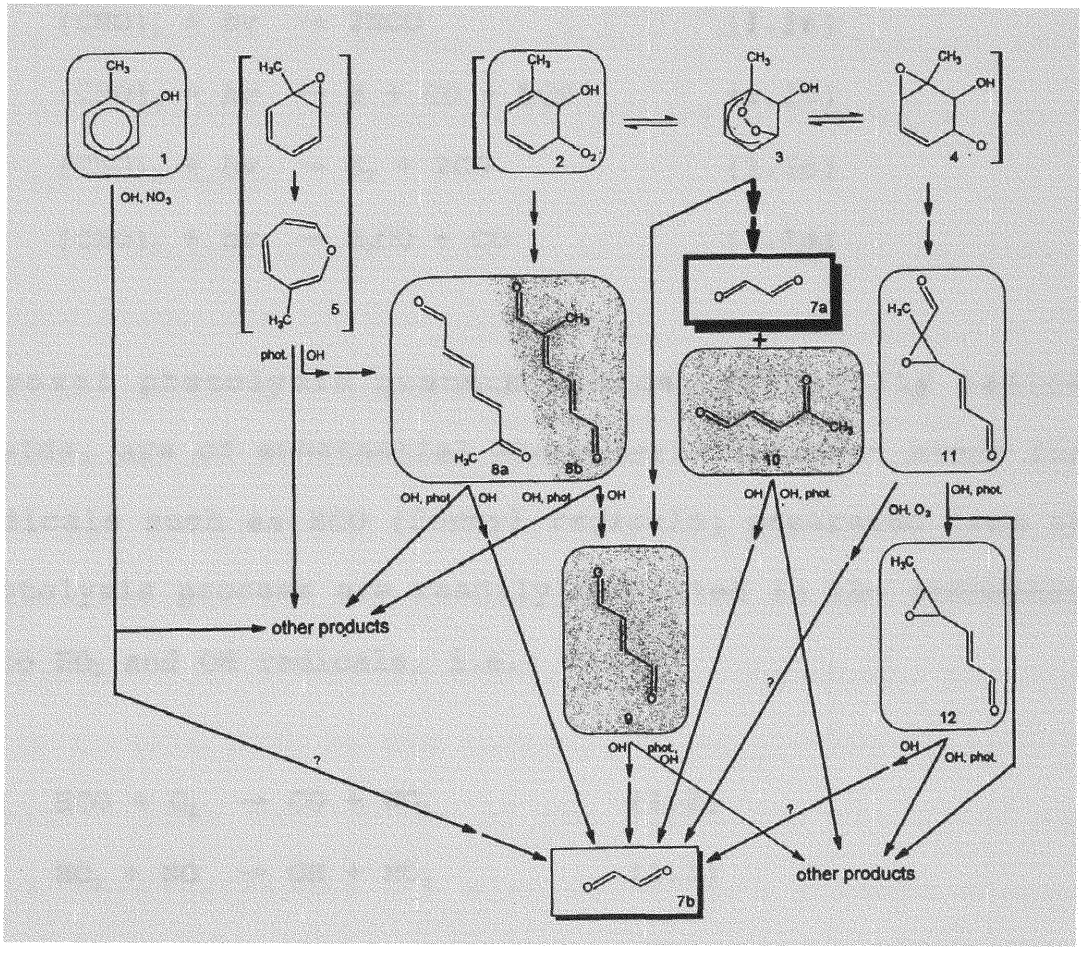

Figure 1.3. Possible pathways for the formation of glyoxal (shaded boxes) from toluene. [Volkamer et al., 2001]

Some of the loss processes of glyoxal are known to be reaction with OH radicals and scavenging by atmospheric droplets. These elimination processes are, however, of little importance. The most important removal process for glyoxal in the troposphere is photolysis. [Zhu et al., 1996] Photolysis of glyoxal can occur through the following pathways [Zhu et al., 1996]:

$$(CHO)_2 + h\nu \rightarrow 2HCO \qquad (1.1a)$$

$$(CHO)_2 + h\nu \rightarrow H + CO + HCO \qquad (1.1b)$$

$$(CHO)_2 + h\nu \rightarrow H_2 + 2CO \qquad (1.1c)$$

$$(CHO)_2 + h\nu \rightarrow H_2CO + CO \qquad (1.1d)$$

Glyoxal photolysis quantum yields, especially radical yields, are of substantial atmospheric interest since free radicals such as HCO (formyl radicals) generated from the photolysis process are readily converted in the atmosphere into HO_2 and OH radicals, i.e.:

$$HCO + O_2 \rightarrow CO + HO_2 \qquad (1.2)$$

$$HO_2 + NO \rightarrow OH + NO_2 \qquad (1.3)$$

These reactions can ultimately speed up photochemical transformations.

Molecular orbital energy level diagram

The most characteristic electronic features of the glyoxal molecule are the free oxygen non-bonding (n) orbitals and the π-orbitals on the C=O groups. To first order, the electronic properties of glyoxal follow from a consideration of the n, π one-electron LCAO MOs.

In Figure 1.4, the n, π one-electron orbitals are drawn with their respective symmetry in the C_2h point-group (the trans conformer of glyoxal). [Drent and Kommandeur, 1972] Although glyoxal can also be in the cis conformation, it is not as prominent.

To zeroth order, the n-orbitals on the different oxygen atoms are of the same energy thus the orbitals can be represented by a symmetric linear combination (a_g) and an antisymmetric linear combination (b_u). Through interaction with each other and with the σ, σ*-orbitals the energies of these orbitals will split making the antisymmetric linear combination b_u lesser in energy. The π-orbitals are also split in this case by the conjugation across the central C-C bond. Upon excitation of the molecule, the $\pi^*_3 \leftarrow n^+$ and $\pi^*_4 \leftarrow n^-$ configurations are electric-dipole allowed whereas $\pi^*_4 \leftarrow n^+$ and $\pi^*_3 \leftarrow n^-$ excitations are dipole forbidden by symmetry. [Drent and Kommandeur, 1972]

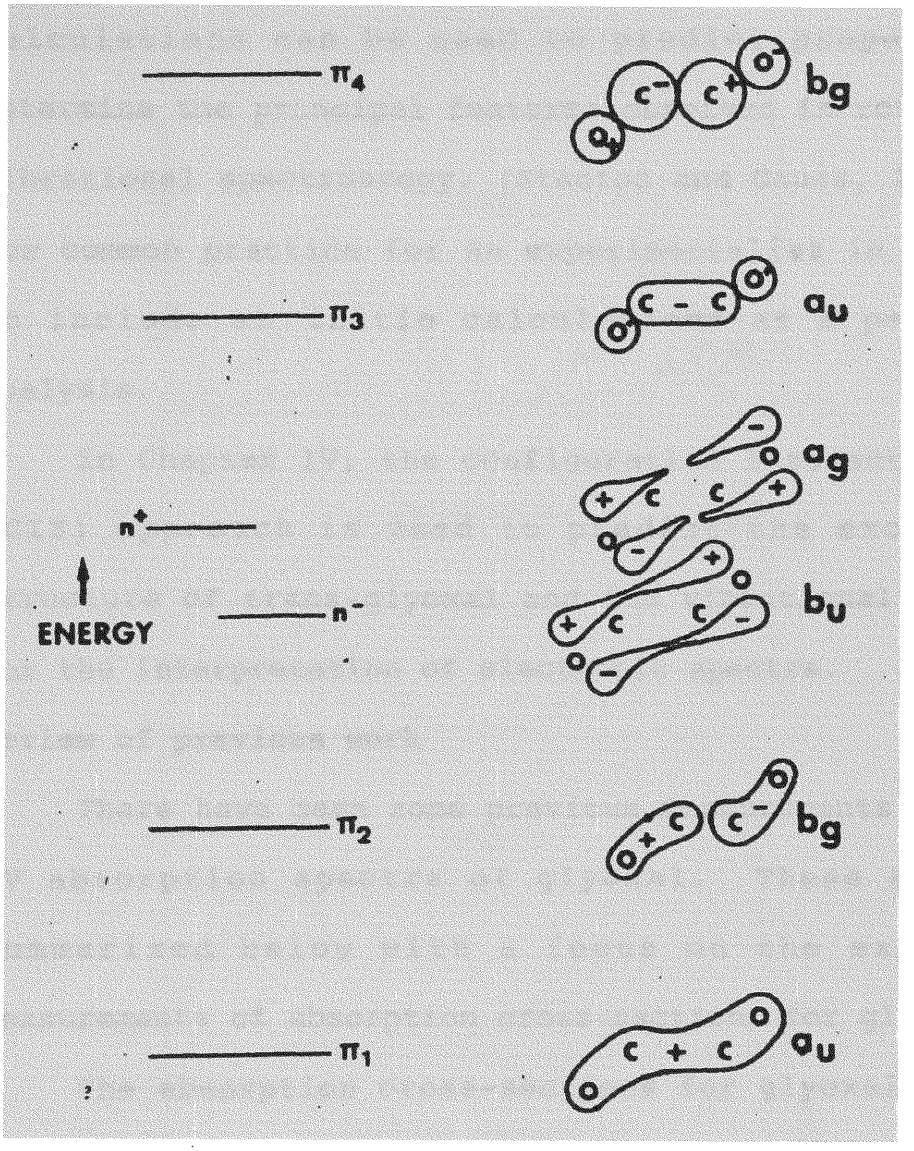

Figure 1.4. Molecular orbitals for trans-glyoxal. [Drent and Kommandeur, 1972]

It is widely recognized that ab initio calculations can be useful in confirming or guiding in assignments in many branches of molecular spectroscopy. When adequate basis sets and correlation treatments are used, such

calculations can be used to predict properties that determine the principal features observed in rotational and vibrational spectroscopy. [Stanton and Gauss, 1996] It is now common practice for an experimentalist in these areas to include ab initio calculations as a part of data analysis.

In Chapter IV, the configuration interaction singles (CIS) approach is used to predict the excited state structure of trans-glyoxal and its vibrational frequencies for the interpretation of electronic spectra.

Review of previous work

There have been some previous measurements of the near UV absorption spectra of glyoxal. These studies are summarized below with a focus on the experimental measurements of absorption cross-sections for glyoxal.

The absorption cross-sections for glyoxal by Plum et al. [1983] were determined by using a Cary 17-D spectrophotometer and known pressures (~3-13 torr measured with an MKS Baratron capacitance manometer). Their published gas-phase glyoxal absorption spectra can be seen in Figure 1.5.

Zhu and coworkers employed excimer laser photolysis for their cross-section measurements. The absorption cross-section of glyoxal at a given photolysis wavelength

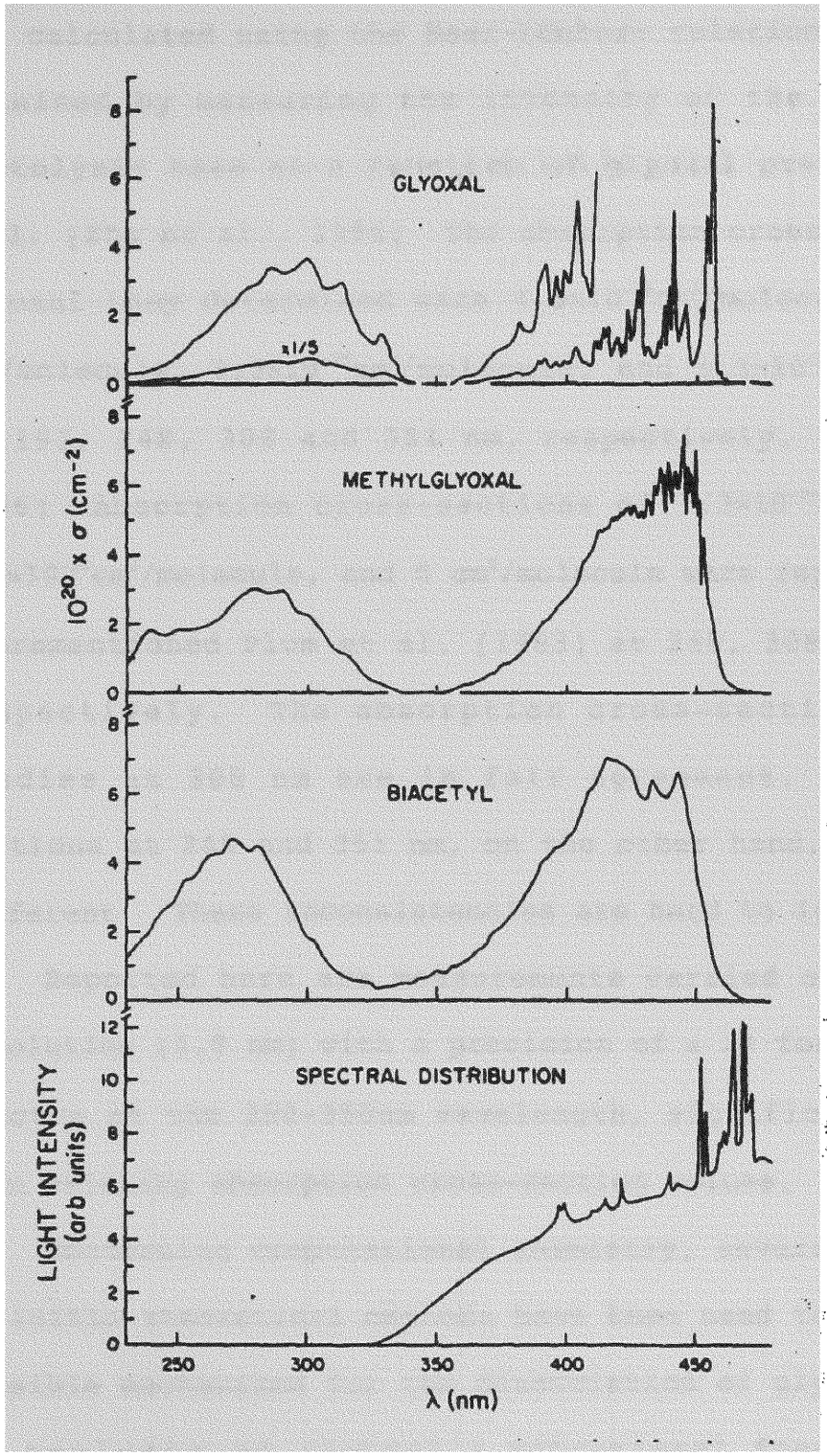

Figure 1.5. (Top) Gas-phase absorption spectra determined for glyoxal by Plum et al., 1983.

was calculated using the Beer-Lambert relation on the data obtained by measuring the intensity of the transmitted photolysis beam as a function of glyoxal pressure in the cell. [Zhu et al., 1996] The absorption cross-sections of glyoxal they determined were 4.8×10^{-19}cm^2/molecule, 1.3×10^{-20} cm^2/molecule, 2.9×10^{-20}cm^2/molecule, and 5.1×10^{-21}cm^2/molecule at 193, 248, 308 and 351 nm, respectively. [Zhu et al., 1996] Absorption cross-sections of 7.3×10^{-21}cm^2/molecule, 2.8×10^{-20}cm^2/molecule, and 0 cm^2/molecule were reported by the aforementioned Plum et al. [1983] at 248, 308 and 351 nm, respectively. The absorption cross-sections of both studies at 308 nm are in fair agreement. The cross-sections at 248 and 351 nm, on the other hand, are largely different. These inconsistencies are hard to ignore.

Reported here are measurements carried out at medium resolution (1.0 nm) with a precision of ± 2% for the glyoxal spectra at the 200-350nm wavelength, significantly better than existing absorption cross-section values.

Concerning computational chemistry, several high-level ab initio theoretical methods have been used to investigate possible mechanisms for the dissociation of glyoxal as well as analysis of glyoxal's vibrational frequencies and electronic transitions for the ground and excited states. A theoretical study of particular interest is the analysis

of the structure and harmonic frequencies of planar conformers of glyoxal in their first excited singlet state by Stanton and Gauss [1996]. Their results using a high level of theory will be reviewed in Chapter IV.

Alternatively, a different level of theory (CIS approach) was used for this thesis. The computational results were instrumental in the investigation, and ultimately the interpretation of, the spectral region of study.

Chapter II

Experimental data analysis

Preparation of glyoxal

Glyoxal is an unstable compound that needs to be either freshly prepared or stored at temperatures of -78°C before use. Some early reports of the production of glyoxal included the oxidation of ethylene with selenium dioxide. [Clavert and Lane, 1953; Carpenter and Foster, 1958] More recent, conventional methods use a derivative precursor of the compound, such as paraglyoxal or glyoxal trimeric hidydrate, as starting materials to obtain glyoxal. Reported below are the two methods that were ultimately attempted.

Plum et. al. [1983] prepared glyoxal by first evaporating a commercially available glyoxal-water solution to dryness under vacuum. Then, after adding and mixing P_2O_5 to the resulting polymer-like material, the α-dicarbonyl was distilled off under vacuum and collected at 77°K. [Plum et al. 1983]

Zhu et al. [1996], on the other hand, produced glyoxal by heating glyoxal trimeric dihydrate in the presence of P_2O_5. [Langford and Moore, 1984] The glyoxal samples were

purified by repeated freeze-pump-thaw cycles and were stored at liquid-nitrogen temperature before use.

The first attempt to prepare glyoxal was based on the method used by Plum and coworkers. A commercially available aqueous solution that was 40% glyoxal [Aldrich] by mass was evaporated to dryness under vacuum using the main manifold. (See Figure 2.1) After drying a paraglyoxal polymer was observed. The polymer was under vacuum and stored in the refrigerator. Two days later the distillation of glyoxal was attempted. A manifold with six valves similar to the one shown in Figure 2.1 was used for the distillation. The paraglyoxal was placed on the far left-hand side and a trap on the far right hand side. P_2O_5 (phosphorus pentoxide) was mixed with the paraglyoxal before heating. The vacuum pump was placed in the middle value. A water bath was used to heat the paraglyoxal. The bath water reached a temperature of 90°C. There seemed to be some initial vaporization of the polymer going on as the temperature increased but then a point was reached where no additional distillation occurred. No useful amounts of glyoxal were obtained by this procedure.

In the next attempt 15ml of the glyoxal-40% water solution was placed in a round bottom flask and the water pumped off on the main manifold. A rubber stopper was

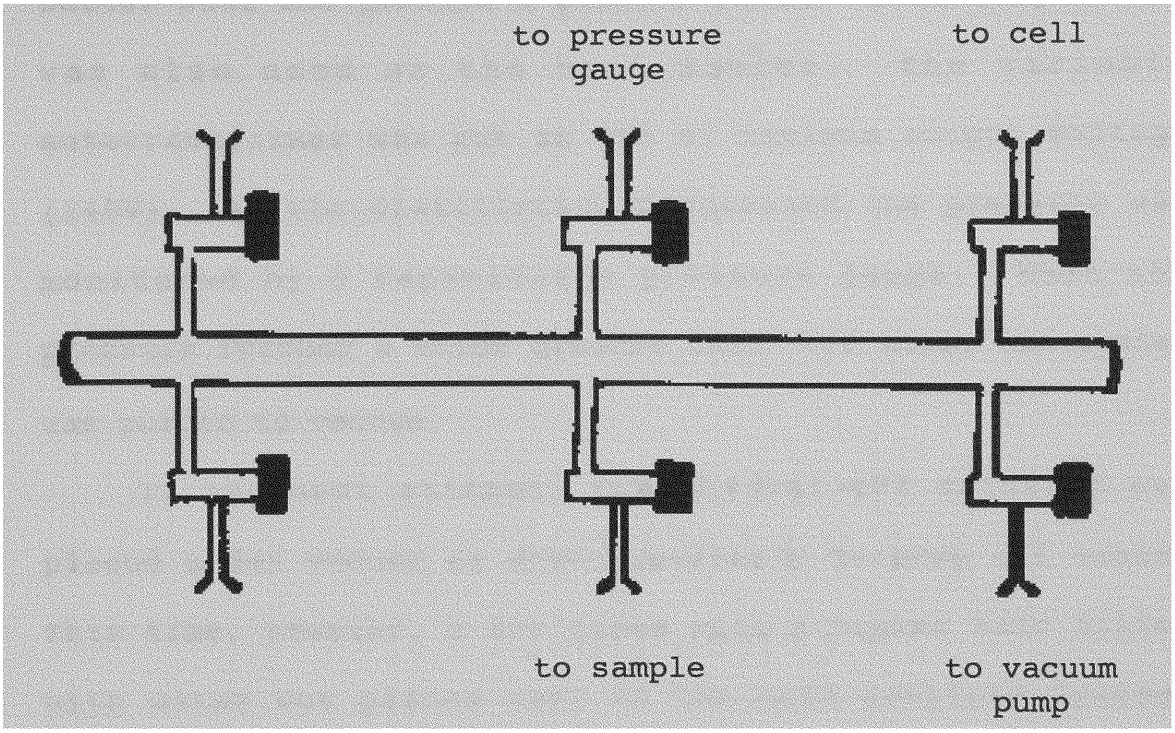

Figure 2.1. Schematic diagram of the gas handling manifold.

joined to a glass connector for the vacuum system and used to stopper the round bottom flask. A few days later, the contents of the round bottom flask were distilled under the hood using the five-valve manifold. Before connecting the round bottom flask an excess of P_2O_5 was mixed into the round bottom flask. During the distillation yellow prisms were seen in the cell (in the trap) consistent with production of glyoxal. It was once again, however, not possible to obtain useful quantities of the compound.

The preparation was attempted again with a new glass stopper, replacing the rubber stopper. This was to give a

better seal and perhaps a greater yield. A heating mantle was also used as the heat source. The variable autotransformer was put at 40% of maximum output voltage (140V). As the distillation progressed the pressure was monitered by a capacitance pressure gauge. When the pressure reached a value greater than ~400 torr, the system was pumped to vacuum.

In the next attempt, the glyoxal-40% solution was placed under vacuum as done previously to pump off water. This time, however, a hot plate with a beaker half filled with water was placed next to the main manifold system. After pumping off the water for hours, the round bottom flask was submerged in the beaker with hot water to ensure as much of the water was pumped off as possible. The paraglyoxal looked different from the previous times. Its appearance was like that of an airy polymer. The crystals formed were white flat crystals with a "naphthalene" like appearance. No phosphorus pentoxide was put into the round bottom flask for the distillation. After being distilled, there seemed to be hot spots created from the heating mantle on the round bottom flask. The contents of the flask appeared to be much browner on one small section of the flask than the rest. The yellow vapor reached almost to the second valve of the manifold set up but not any

further. The cell in the trap was checked frequently but the yellow crystals seen in the first attempt was never seen. The residue left behind in the round bottom flask appeared to be just the burnt glyoxal.

Because of the lack of success in obtaining glyoxal from the aqueous solution, the next attempt to prepare glyoxal was based on the method of Zhu and coworkers. Five grams of glyoxal trimeric dihydrate [Aldrich] and 2.5 grams of phosphorus pentoxide were placed in the round bottom flask. A different distillation apparatus was also set up. (See Figure 2.2) The flask was heated for approximately 40 minutes (variable autotransformer at 40%) when a pale yellow crystalline product was observed in the collection round bottom flask.

Based on the apparent success of this procedure the method was carried out a second time using fifteen grams of the glyoxal trimeric dihydrate along with seven grams of phosphorus pentoxide. A greater yield was obtained. An IR cell was filled with the product and a spectrum was taken. (See Figure 2.3) The peak intensities and locations for glyoxal were compared to the experimentally known values. The spectrum of the product was consequently determined to be glyoxal. The same cell was also filled with benzene, used as a reference spectrum. (See Figure 2.4)

Apparatus

Absorption measurements were made on a Shimadzu UV-2101 PC (Zenith Data System) scanning spectrophotometer. The spectrophotometer is a double beam instrument capable of obtaining spectra in the wavelength region 190-800 nm, at a resolution of 0.1 nm in the UV-visible spectral region. The sample compartment of the spectrophotometer was modified to fit a cylindrical gas absorption cell.

The gas absorption cell was constructed by attaching a pair of one-inch diameter Supracil quartz windows to both ends of a 10 cm length, 25 mm diameter glass tube. A glass stopcock was attached to the body of the cell to allow filling of the cell on a vacuum manifold.

Other glassware, such the gas handling manifolds and the distillation set up, were thoroughly cleaned with nitric acid, a soap solution, water, and deionized water, and then dried before use.

A diagram of the experimental apparatus is given in Figure 2.5.

Test of the apparatus

To check that the instrument is functioning correctly, the Shimadzu UV 2101 spectrophotometer has a number of self-testing sequences that are run automatically at start-up. Due to the nature of the experiments, however,

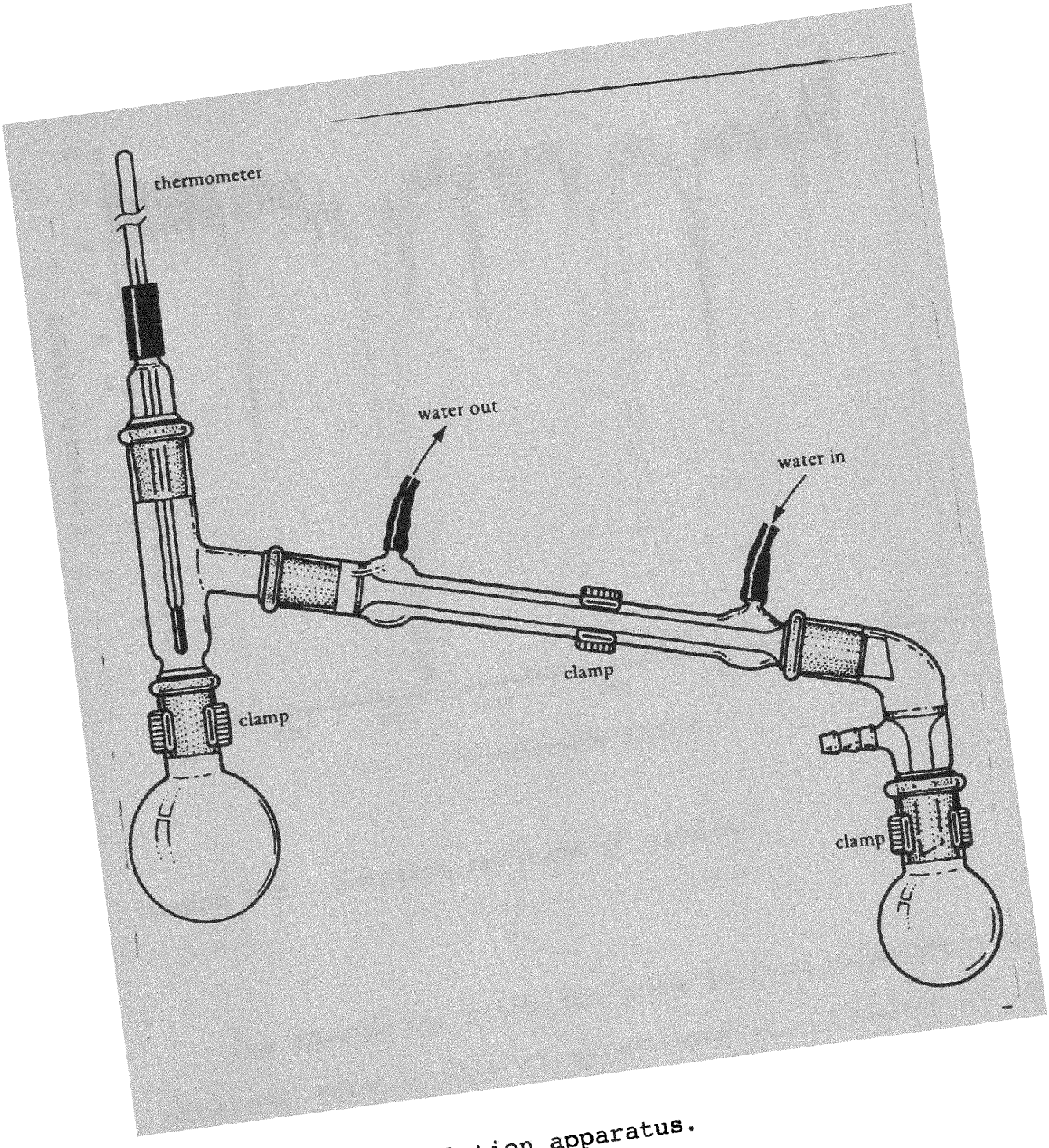

Figure 2.2. Distillation apparatus.

additional tests of the instrument were carried as discussed below.

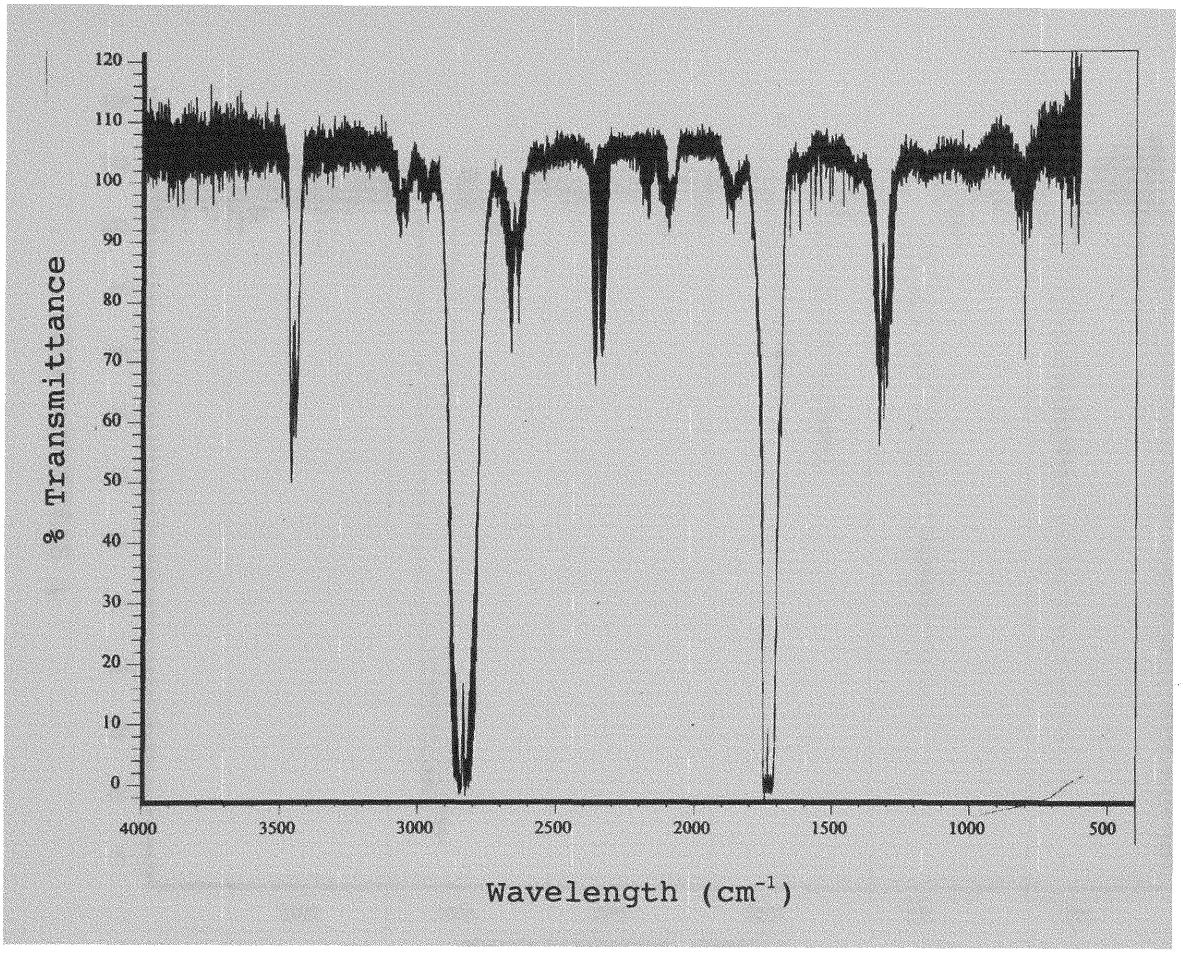

Figure 2.3. Infrared spectrum of glyoxal.

The absorption cross sections in this experiment are obtained from a plot of absorbance vs. pressure of the absorbing gas. Absorption linearity was tested by plotting absorbance vs. concentration for a series of potassium dichromate solutions. A stock solution of approximately 200mg/l potassium dichromate was prepared and diluted to volume with a 0.05 M aqueous potassium hydroxide solution. Serial dilutions of this stock solution were prepared with

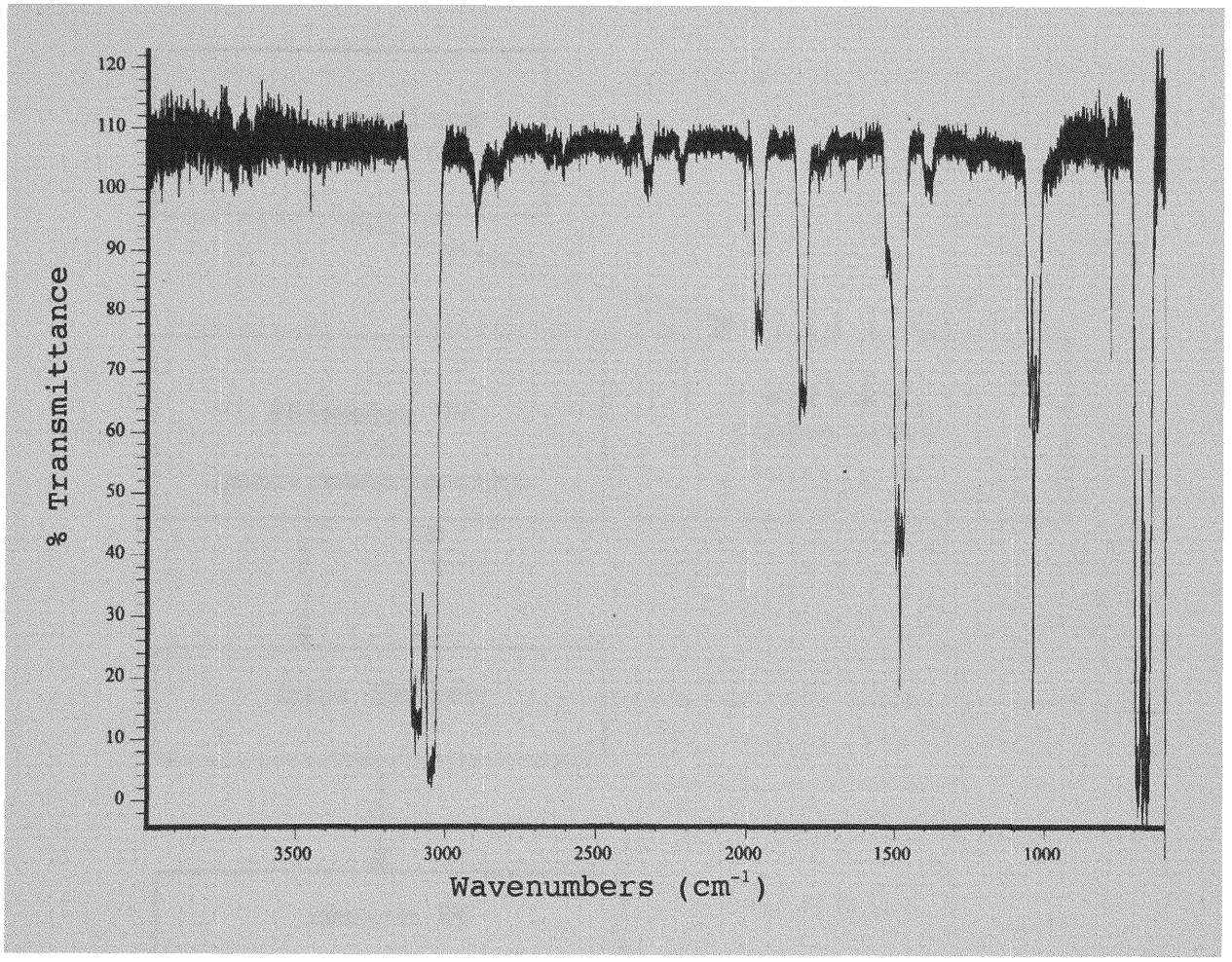

Figure 2.4. Infrared spectrum of benzene.

concentrations from 10-50 mg/l. Absorbance was measured at 320 nm and a spectral bandwidth of 1.0nm. A plot of these intercept, and correlation coefficient for the data showed that no deviations from Beer's law occurred for absorbances in the range of 0-2.5 absorption units.

Wavelength calibration

Two methods were performed for checking the wavelength

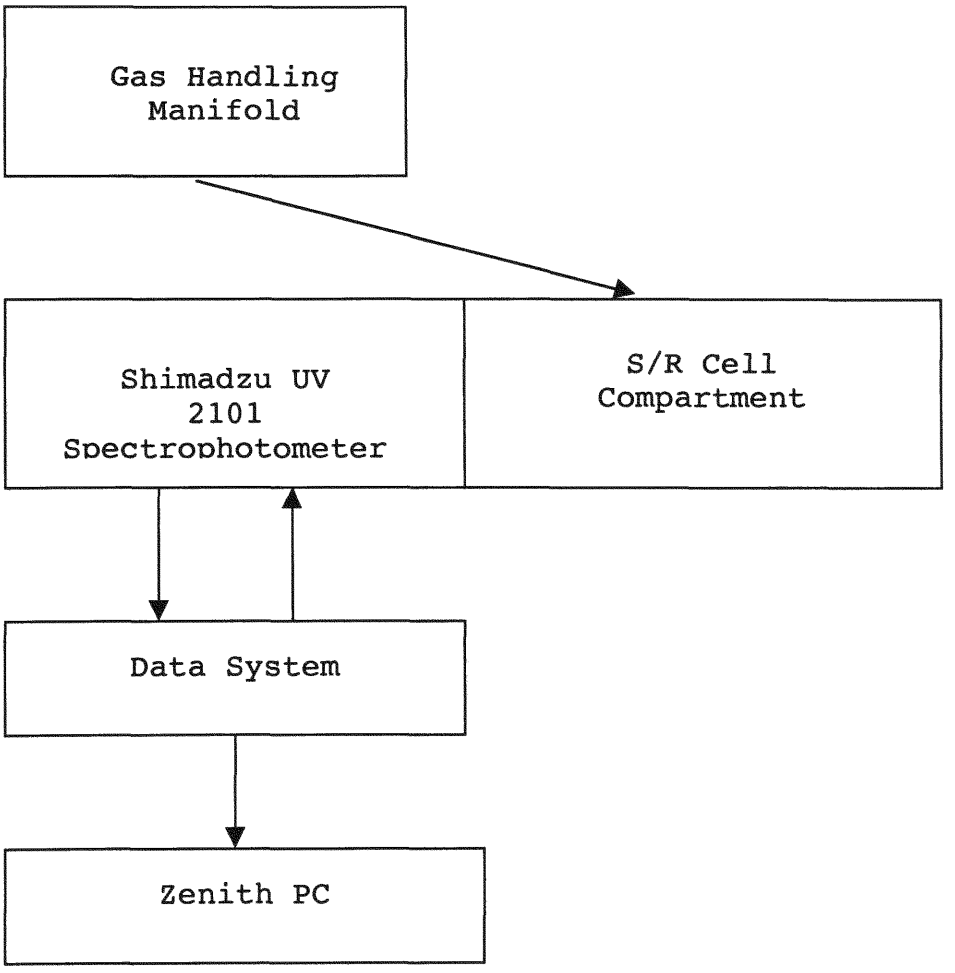

Figure 2.5. Schematic diagram of the experimental apparatus.

calibration of the spectrophotometer. They were instrument self check and the measurement of benzene vapor spectrum.

In the instrument self test, the Shimadzu UV 2101 spectrophotometer uses the emission lines of the deuterium

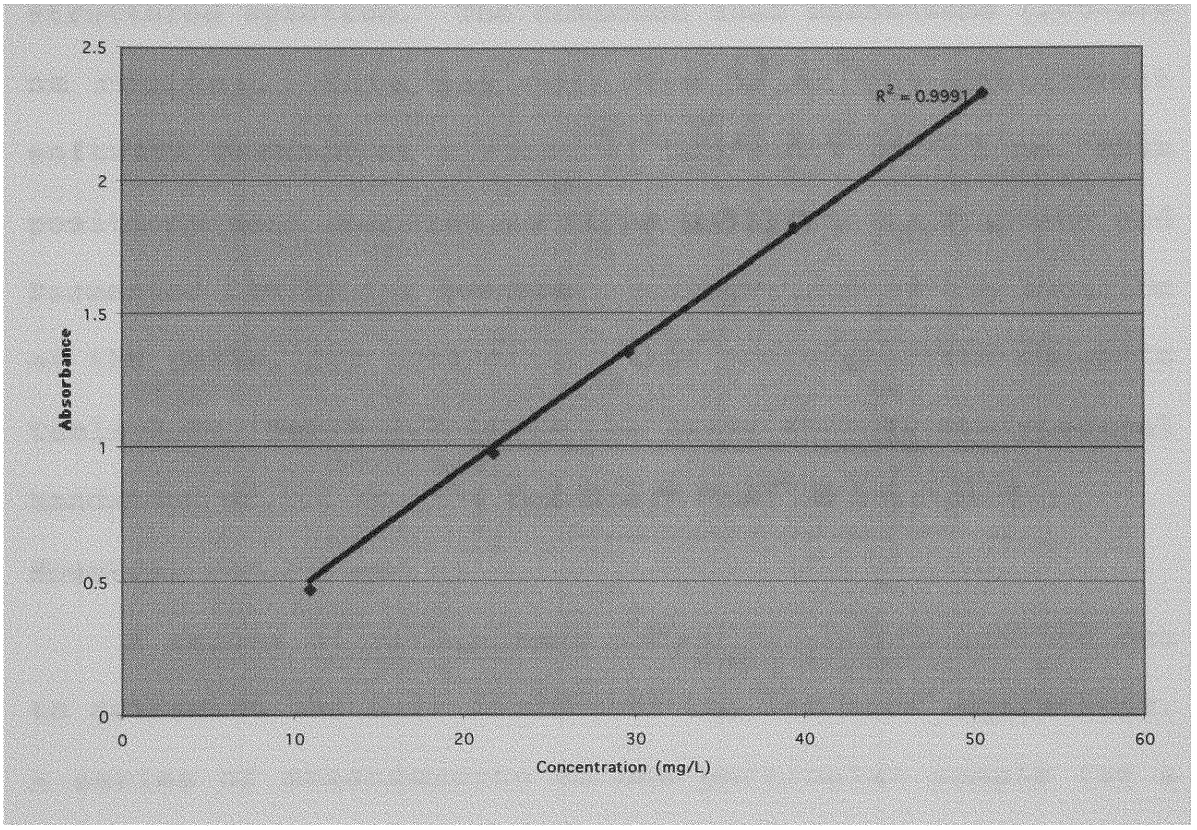

Figure 2.6. Absorbance vs. concentration for the potassium dichromate calibration solutions.

lamps, or overtones of these lines, whose wavelengths are known. The measured values for wavelength are compared with the known values. When turning on the instrument, any unacceptable deviation from these values results in the instrument requesting troubleshooting.

A second calibration test was carried out by measuring the vapor phase spectrum of a compound possessing a highly

structured spectrum. The compound used wasbenzene (200-270 nm region). Data was obtained using the instrument software package at a spectral bandwidth of 0.2 nm. Peak positions were compared to those published by Atkinson and Parmenter [1978] for benzene. A comparison of the location of the peaks, for this calibration procedure, are shown in Table 2.1. Table 2.2 lists the peaks seen at the spectral bandwidth of 1.0 nm (the parameter used in this study).

Spectral resolution

A series of preliminary experiments were carried out to determine the best conditions for the main experiments. A series of measurements on one particular sample (at a pressure of 100 Torr) were performed. In these measurements the sample was viewed at different values of spectral resolution and instrument response time. It was decided, based on the results, that the best spectral resolution for the measurements was 1.0 nm. This is appropriate for an absorption spectrum containing no sharp structured features. The relationship in the determining scan rate is:

$$\text{Scan rate} < \text{Band width/response time.} \quad (2.1)$$

Based on this relationship a scan rate of 0.91 nm/sec was

Table 2.1

Comparison of Benzene Peak Location

Peaks	Location[a] (cm^{-1})	Location[b] (cm^{-1})
1	37481.6	37453.2
2	38522.5	38432.0
3	38611.3	38580.2
4	39038.5	39062.5
5	39534.6	39494.5
6	39638.0	39745.6
7	40131.9	40160.6
8	40456.7	40420.4
9	40968.5	40916.5
10	41165.3	41186.2
11	41254.1	41254.1
12	41478.6	41356.5
13	41924.7	42052.1
14	42298.0	42265.4
15	43009.3	42992.3
16	43215.7	43177.9

(a)From Atkinson and Parmenter [1978]
(b)Shimadzu instrument

Table 2.2

Location of Benzene Peaks at 0.1 nm Bandwidth (Parameter Used in Study)

Peak	Location (cm^{-1})
1	37453.2
5	39447.7
7	40322.6
12	41322.2
13	42194.1
15	42918.5

selected. A number of different sampling intervals were also used. The spectrum could be satisfactorily reproduced using a spacing of 0.5 nm between adjacent data points.

Data acquisition and analysis

The purpose of the experiments was to obtain accurate room temperature absorption cross sections for glyoxal at the 280 nm wavelength. The steps involved in the data acquisition, transfer, and analysis procedure are outlined in Table 2.3. This involved measurement of experimental absorbances as a function of wavelength and pressure of absorbing gas, and conversion of this data into absorption cross section values.

Table 2.3

Summary of the Data Analysis Process

Step	Program
Measure spectrum	SPECDATA.BAS
Transfer data to Zenith P.C.	DATATRAN.BAS
Convert data to absorbances	DATARED.BAS
Align data	PLOTDATA.BAS
Combine data into a single file	PLOTSUM.BAS
Calculate absorption cross-sections	DATAANAL.BAS
Combine cross-sections into a single file	SUMMARY.BAS

The experimental data was obtained on a Shimadzu UV 2101 scanning spectrophotometer interfaced to a PC (Zenith Data System). The experimental conditions (i.e. wavelength range and other operating conditions) are given in Table 2.4. All spectra were measured at room temperature (~20°C) at a spectral bandwidth of 1.0mm, a scan rate of 0.91 nm/sec, and a sampling interval of 0.5 nm/data point.

Table 2.4

Operating conditions for the Spectrophotometer

Spectral Bandwidth	1.0 nm
Scan Rate	0.91 nm/sec
Spacing between data points	0.5 nm

Experimental data was obtained by first running a baseline spectrum with the empty reference gas absorption cell in place, then measuring the absorption spectrum over the particular wavelength range in the following sequence:

B1 = Empty sample cell with a pressure of 0 Torr (2.2a)

S1, S2 = cell filled with absorbing gas at (2.2b)

a known pressure of glyoxal

B2 = Empty sample cell with a pressure of 0 Torr (2.2c)

A spectrum was measured with the empty sample cell. The cell was then filled with glyoxal at a known pressure and measured. Duplicate measurements were made of the filled cell. The cell was then evacuated and a second blank spectrum was run.

The sequence of four spectra (B1, S1, S2, B2) for the particular wavelength range and an absorbing gas pressure were stored as a sequence of data point pairs containing the experimental wavelength and absorbance. The data for each spectrum were temporarily stored on diskette in four separate files, named BXYYY for the blanks. X was assigned based on the number of samples run that day and varied from one to five. The YYY stood for the first letter of the month the spectra was run followed by the day. The samples were named FX1YYY and FX2YYY, where X depended on the sequence that the sample was run that day and the YYY for the samples were labeled following the same format as the blanks. The actual acquisition of data was done following the sequence in Equations 2.2a,b,c.

Date analysis

The next step in the data analysis consisted of taking the four experimental files (B1, S1, S2, B2) and converting them into a single file of experimental wavelengths and absorbances. This was accomplished using the program DATARED.BAS, a data reduction program.

For each wavelength an experimental absorbance was calculated using the relationship:

$$A = [(S1 + S2) - (B1 + B2)]/2 \qquad (2.3)$$

where A is the experimental absorbance. By subtracting the blank spectrum (B1+B2) from the sample spectrum (S1+S2), a correction was made for a possible drift in the instrument baseline. The result of the above process was a reduced data set of absorbances.

Absorbance/pressure vs. wavelength were plotted using PLOTDATA.BAS for a series of runs. Those runs that showed evidence of degradation or baseline drift were discarded. Once a set of reliable experimental data had been obtained cross-section calculations were initiated.

Cross-section calculation

The absorption cross-section for glyoxal could be calculated. This was accomplished by using the method of linear least squares to find the best fitting line to the

data. The absorption cross-section, σ (in units of cm^2-$molecule^{-1}$) is given by the equation;

$$\sigma = (2.303/l)(dA/dN) \qquad (2.4)$$

where l is the path length of the cell (9.803cm). dA/dN is related to dA/dP, the slope of the best fitting line in the plot of absorbance vs. pressure, by the relationship:

$$dA/dP = (1.379\times10^{-3}\ molecule/torr\text{-}cm^3)(dA/dN) \qquad (2.5)$$

where the conversion factor between dA/dP and dA/dN is calculated assuming all pressures are reported at T= 298.15° K.

The data for individual wavelengths can be plotted to check the reliability of the data. An example set of the data is shown in Figure 2.7. The absorption cross-section σ, calculated by the above procedure, is the coefficient seen when Beer's law is written in the form:

$$I/I_o = \exp(-\sigma N l) \qquad (2.6)$$

where I_o is the initial intensity, I is the light intensity after passing through the cell, σ is the absorption cross-

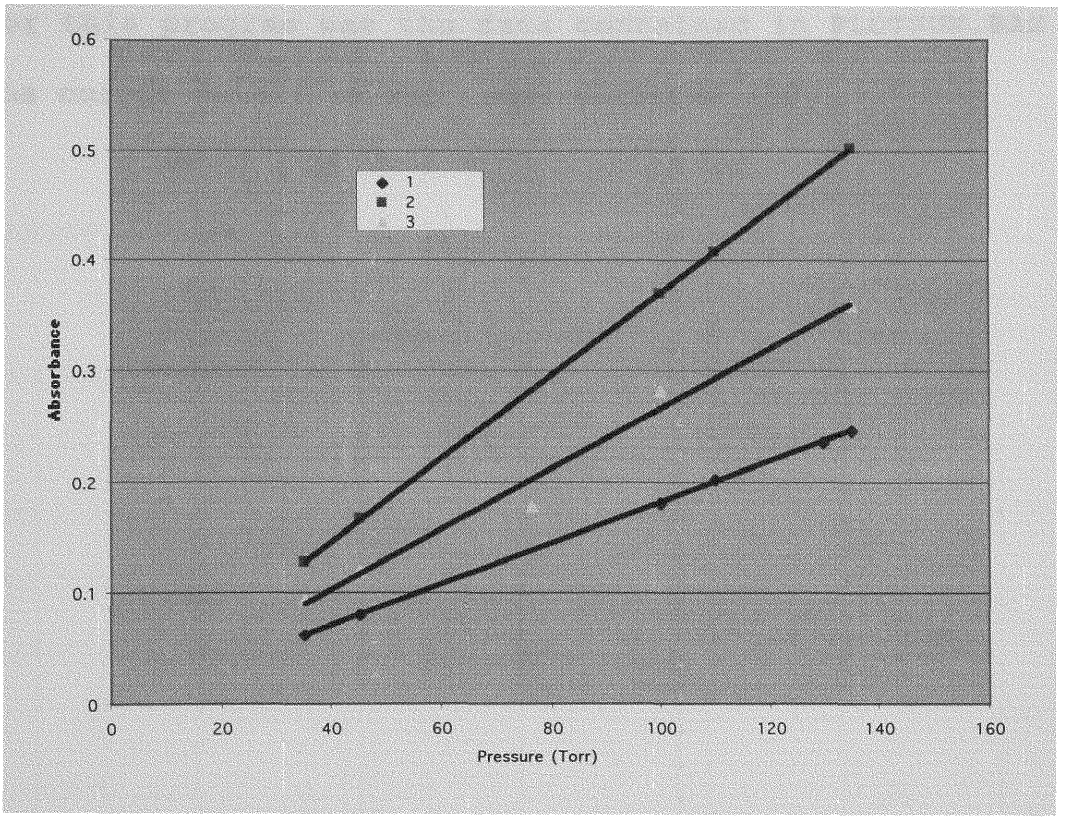

Figure 2.7. Absorbance vs. pressure for glyoxal at (1) 330 nm, (2) 310 nm, and (3) 270 nm.

section discussed earlier, N is the number density of absorbing gas molecules in units of molecules-cm^{-3}, and l is the path length in cm.

The calculations of the absorption cross-sections were carried out in the program DATAANAL.BAS. The input data

for this program was the data contained in PLOTSUM.BAS and the output data file was named GLYSHORT.ASC.

Chapter III

Experimental Results

Summary of results

The final results for the absorption cross-sections for glyoxal, obtained from the experimental data, are shown in Figure 3.1. The complete set of absorption cross-section values as a function of wavelength is presented in Appendix A.

Comparison with previous works

The results from the measurements of the near UV absorption spectra of glyoxal are represented as absorption cross-sections. The cross-sections are given at a spacing interval of 0.5 nm and at a temperature of 298.15 K. The range of wavelengths for which the values are reported is 200-350 nm. Table 3.1 shows a comparison between the results obtained in this study, Plum et al. [1983], and Zhu et al. [1996].

The glyoxal absorption cross-sections at 308 nm are all in good agreement. The cross-section at 248 nm reported by Zhu et al. [1996] is larger than those determined by both this study and Plum et al. [1983]. The values reported in this thesis, and those found by Plum and coworkers, however, are very similar.

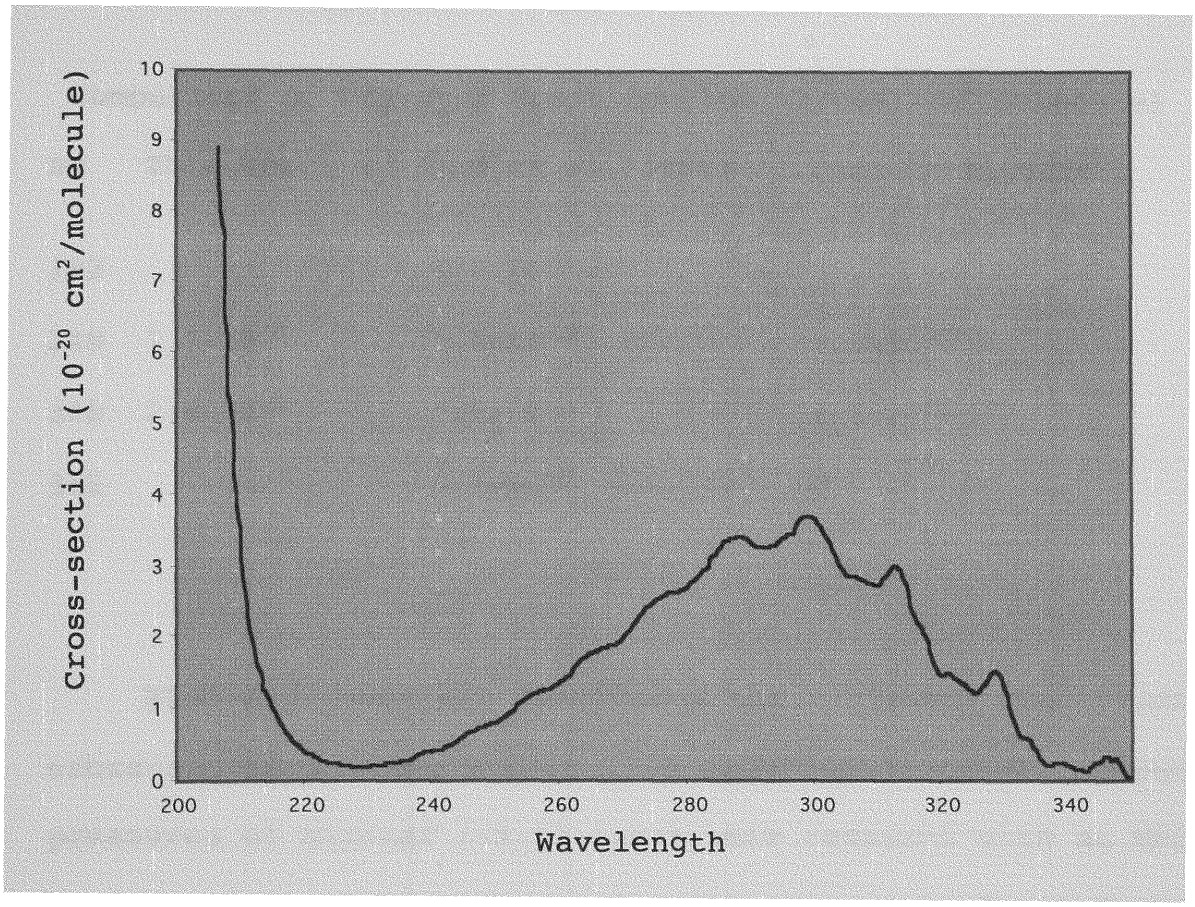

Figure 3.1. Spectra of glyoxal.

The wavelength region in this study, that is 200-350 nm, did not include the other two wavelengths listed. However, it should be mentioned that at the 351 nm wavelength, Zhu et al. [1996] reports a glyoxal cross-section significantly larger than Plum et al. [1983].

Table 3.1

Comparison of Previous Cross-Section Values (cm^2/molecule)

nm	This Work	Zhu et al.(1996)	Plum et al.(1983)
193		4.8×10^{-19}	
248	7.7×10^{-21}	1.3×10^{-20}	7.3×10^{-21}
308	2.8×10^{-20}	2.9×10^{-20}	2.8×10^{-20}
351		5.1×10^{-21}	0

Plum and coworkers determined their glyoxal absorption cross-sections using a Cary 17-D spectrophotometer. Known pressures of glyoxal (~3-13 torr) were measured with an MKS Baratron capacitance manometer. The experimental apparatus used in the study for this thesis were similar but the range of pressures of glyoxal are larger, that is ~26-135 torr. Zhu et al. (1996), on the other hand, employed excimer laser photolysis at 193, 248, 308 and 351 nm in combination with cavity ring-down spectroscopy. Zhu et al. (1996) claim they checked the purity of the glyoxal, repeatedly measured its absorption cross-sections at the reported photolysis wavelengths and have confidence in their results.

As was noted above, however, the results for both studies are similar. Further studies should be conducted to verify what the cross-section measurements are at the wavelengths with conflicting values.

Chapter IV

Computational Theoretical Background

Presently, it is possible to run computational programs in order to obtain information pertaining to molecules. Electronic structure calculations have become a common tool to predict the equilibrium geometry of molecules. In fact, the total energy of a molecule can be defined by a potential energy surface. The points on this potential surface represent solutions to questions that can help in the prediction of chemical structures. For this thesis, calculations were run to explain what is happening to the glyoxal molecule during photodissociation, that is how it breaks apart and the interpretation of the region of study.

The Schrodinger Equation

Using the laws of quantum mechanics, the energy and other related properties of a molecule may be obtain by solving the Schrodinger equation [Atkins and Freidman, 1997]:

$$H\Psi = E\Psi \qquad (4.1)$$

The operator in Equation (4.1) that returns the system energy, E, as an eigenvalue is called the Hamiltonian operator, H. This Hamiltonian operator typically takes into account five contributions to the total energy of a molecule: the kinetic energies of the electrons and nuclei, the attraction of the electrons to the nuclei, and the interelectronic and internuclear repulsions. [Cramer, 2002] Placing the Hamiltonian into mathematical notation:

$$H = -\sum(h/2\pi)^2/2m_e\nabla^2_i - \sum(h/2\pi)^2/2m_k\nabla^2_k - \sum\sum e^2Z_k/r_{ik} + \sum e^2/r_{ij} + \sum e^2Z_kZ_l/r_{kl} \quad (4.2)$$

where i and j run over electrons, k and l run over nuclei, h is Planck's constant, m_e is the mass of the electron, m_k is the mass of nucleus k, ∇^2 is the Laplacian operator, e is the charge on the electron, Z is an atomic number, and r_{ab} is the distance between particles a and b.

The Born-Oppenheimer approximation

The Hamiltonian in Equation (4.2) contains pairwise attraction and repulsion terms implying that no particle is moving independently of all of the others, i. e. there is an interdependency. As a result, accurate wavefunctions for such systems are extremely difficult to express because of the correlated motions of particles, and solving the

Schrodinger equation even for a simple molecule is not an easy task. This is where the Born-Oppenheimer approximation becomes useful. The Born-Oppenheimer approximation is based on the fact that, under typical physical conditions, the nuclei of molecular systems are moving much more slowly than the electrons. For practical purposes, the electrons react essentially instantaneously to changes in nuclear position. Thus, the electron distribution within a molecular system depends on the positions of the nuclei, and not on their velocities. [Foresman and Frisch, 1996] Put another way, the electrons can be described as occurring in a field of fixed nuclei.

Hartree-Fock theory

D. R. Hartree introduced a method to calculate the energy and the ground state wavefunction of an atom in 1928. [Hartree, 1928] In this method, the Schrodinger equation is examined in the context of a one-electron Hamiltonian. As such, the only terms in the Hamiltonian are the one-electron kinetic energy and nuclear attaction terms. Moreover, the operator is 'separable' and may be expressed as:

$$H = \Sigma h_i \qquad (4.3)$$

where N is the total number of electrons and h_i is the one-electron Hamiltonian defined by;

$$h_i = -1/2\nabla_i^2 - \Sigma Z_k/r_{ik} \qquad (4.4)$$

where M is the total number of nuclei. The eigenfunction of the one-electron Hamiltonian defined in the above Equation (4.4) must satisfy the corresponding one-electron Schrodinger equation:

$$h_i\psi_i = \varepsilon_i\psi_i \qquad (4.5)$$

Since the Hamiltonian operator defined by Equation (4.3) is separable, its many-electron eigenfunctions can be constructed as products of one-electron eigenfunctions, i.e.

$$\Psi_{HP} = \psi_1\psi_2\cdots\psi_N \qquad (4.6)$$

The Hamiltonian defined by Eqs. (4.3) and (4.4) does not include interelectronic repulsion. This computation depends not on one electron, but instead on all possible (simultaneous) pair-wise interactions. The Hartree-product wavefunction Ψ_{HP} can be useful in computing energies from

the correct Hamiltonian. That is, the goal is to find orbitals that minimize $\langle \Psi_{HP} | H | \Psi_{HP} \rangle$. By applying variational calculus, one can show that each such orbital ψ_i, is an eingenfunction of its own operator h_i defined by;

$$h_i = -1/2\nabla_i^2 - \sum Z_k/r_{ik} + V_i\{j\} \qquad (4.7)$$

where the final term represents an interaction potential with all of the other elections occupying orbitals {j} and may be computed as;

$$V_i\{j\} = \sum \int \rho_j/r_{ij} \; dr \qquad (4.8)$$

where ρ_j is the charge (probability) density associated with electron j. [Cramer, 2002] The repulsive third term on the right hand side of Equation (4.7) is thus, exactly analogous to the attractive second term, except that the nuclei are treated as point charges, while electrons, being treated as wavefunctions, have their charge spread out, requiring an integration over all space. [Cramer, 2002] In short, the field seen by electron i, depends on the orbitals of the other electrons. Thus, the equation is nonlinear and must be solved iteratively.

Hartree proposed an iterative 'self-consistent field' (SCF) method to finesse this problem. In the first step of the SCF process, one initially guesses the wavefunctions for all of the occupied MOs constructing the necessary one-electron operators, h. Solution of each differential equation (4.5) provides a new set of wavefunctions. These presumably more accurate wavefunctions are used to form anew the one-electron Hamiltonians and ultimately determine each necessary ρ. The process is repeated to obtain a still better set of wavefunctions. At some point, the difference between a newly determined set and the immediately preceeding set falls below some threshold criterion, and the final set of wavefunctions is referred to as the 'converged' SCF orbitals.

One problem with the Hartree wavefunction is that they do not involve spin and are not anti-symmetric with respect to electron exchange. [Atkins and Friedman, 1997] This was addressed by J. C. Slater and V. Fock by including spin orbitals and the effect of electron exchange. They stated that the product of the molecular orbital and spin function must not be neglected and that it is essential to take linear combinations of anti-symmetric products of spin orbitals. This type of self-consistent field calculations

received the name Hartee-Fock calculation. [Atkins and Friedman, 1997]

In this thesis, restricted calculations were performed, that is, calculations of a closed shell nature to analyze the excited states of glyoxal. Two different types of basis sets were used in these calculations. Below is a discussion, which describes basis sets used for the calculations.

Electron spin

All electrons have either of two types of spin, up (+1/2) or down (- 1/2). Molecular calculations can either be closed shell or open shell. Closed shell calculations are referred to as restricted calculations and used doubly occupied orbitals that hold two electrons having opposite spins. Open shell calculations, better known as unrestricted calculations, use separate orbitals for the spin up and the spin down electrons. The two spin functions, α and β, are defined as follows:

$$\alpha\ (+1/2) = 1 \qquad \alpha\ (-1/2) = 0 \qquad (4.7a)$$

$$\beta\ (+1/2) = 0 \qquad \beta\ (-1/2) = 1 \qquad (4.7b)$$

The function is 1 when an electron is spin up and the β function is 1 when the electron is spin down. The notation

$\alpha(i)$ and $\beta(i)$ designate the values of α and β for electron i. To include the electron spin in the electron wavefunction, the molecular orbital function is multiplied by either α or β. The resultant product of the molecular orbital in a spin orbital is defined as a spin orbital, a function of both the electron's location and it's spin.

Basis sets

A basis set is the mathematical description of the orbitals within a system (which in turn combine to approximate the total electronic wavefunction), used to perform the theoretical calculation. [Foresman and Frisch, 1996] In general, the larger the basis set the more accurate the approximation to the orbitals becomes.

Standard basis sets express the molecular orbitals as linear combinations of a predefined set of one-electron functions known as basis functions. These basis functions are usually centered on the atomic nuclei and so resemble atomic orbitals. Each individual molecular orbital is defined as:

$$\phi_i = \sum c_{ui}\chi_\mu \qquad (4.8)$$

where the coefficients $c_{\mu i}$ are known as the molecular orbital expansion coefficients. The basis functions, $\chi_1 \cdots \chi_N$,

are chosen to be normalized. Moreover, χ_μ refers to an arbitrary basis set in the same way, ϕ_i, refers to an arbitrary molecular orbital. There are two types of commonly used basis functions: Slater-type orbitals (STOs) and Gaussian-type orbitals (GTOs).

Gaussian-type functions are used as basis functions in the Gaussian suite of programs and are defined as follows [Atkins and Freidman, 1997]:

$$g(\alpha,r) = cx^n y^m z^l e^{-\alpha r^2} \qquad (4.9)$$

where r is the position vector (x,y,z) and α is a constant determining the size (radial extent) of the function. In a Gaussian function, $e^{-\alpha r^2}$ is multiplied by powers (possibly 0) of x,y,z and a constant for normalization, so that, $\int g^2 = 1$. The three gaussian functions (s, py and dxy types, respectively) are:

$$g_s(\alpha,r) = (2\alpha/\pi)^{3/4} e^{-\alpha r^2}, \qquad (4.10a)$$

$$g_y(\alpha,r) = (128\alpha^5/\pi^3)^{1/4} y e^{-\alpha r^2}, \qquad (4.10b)$$

$$g_{xy}(\alpha,r) = (2048\alpha^7/\pi^3)^{1/4} xy e^{-\alpha r^2}, \qquad (4.10c)$$

Linear combinations of primitive gaussian like these are used to form the actual basis function; the latter are called contracted Gaussians and have the form [Foresman and Frisch, 1996]:

$$\chi_\mu = \sum d_{\mu p} g_p \qquad (4.11)$$

where the $d_{\mu p}$'s are fixed constants within a given basis set. This results in the following expansion for molecular orbitals:

$$\phi_i = \sum c_{\mu i} \chi_\mu = \sum c_{\mu i} (\sum d_{\mu p} g_p) \qquad (4.12)$$

Basis set effects

Minimal basis sets contain the minimum number of basis functions needed for each atom. A way to improve the minimal basis set is to increase the number of basis sets per atom. Split valence basis sets, such as 3-12G and 6-31G, have two (or more) sizes of basis function for each valence orbital. The adopted nomenclature is a guide to the contraction scheme. The first number indicates the number of primitives used in the contracted core function, while the numbers after the hyphen indicate the number of primitives used in the valence functions; e.g. if there are

two such numbers, it is a valence-double-zeta basis, if there are three, valence-triple-zeta. [Cramer, 2002]

Atomic orbitals can change in size and shape depending on the neighboring atom when a bond is formed. In order to account for the distortions caused by bond formations, basis functions can be included to represent the orbitals of higher values of 1. The distortion of a 1s-orbital can be described by the addition of a p-type basis function, and a d-type function can describe distortions of p-orbitals. Thus, 6-31G(d) indicates that it is the 6-31G basis set with d-type functions added to heavy atoms. Along the same lines, the polarized basis set 6-31G(d,p) adds p-type functions to hydrogen atoms in addition to the d-type functions on heavy atoms.

Diffuse functions

Diffuse functions, also known as augmented functions (designated by + or ++), allow orbitals to occupy a larger region of space. The 6-31+G(d) basis set is the 6-31G(d) basis set with diffuse functions added to heavy atoms while the double plus version, 6-31++G(d), adds diffuse functions to the hydrogen atoms as well.

Basis sets with diffuse functions are important for systems where electrons are relatively far from the nucleus, i.e. systems in their excited states. [Foresman and Frisch,

1996] Since the goal of this thesis was to model the excited spectra of glyoxal, the 6-31+G(d) seemed the logical basis set of choice. For better accuracy, the triple-zeta basis set was used as well. This was done in the hopes of increasing the flexibility of the representative glyoxal molecule and to improve the outer valence region.

Electron correlation

It is common knowledge that the Hartree-Fock theory provides an inadequate treatment of the correlation between the motion of the electrons within a molecular system, especially those between electrons of opposite spin. When Hartree-Fock theory fulfills the requirement that $|\Psi|^2$ be invariant with respect to the exchange of any two electrons by anti-symmetrizing the wavefunction, it automatically includes the major correlation effects arising from pairs of electrons with the same spin. [Foresman and Frisch, 1996] This is better known as exchange correlation. Under Hartree-Fock theory, however, the motion of electrons of opposite spin remains uncorrelated. A method such as configuration interaction, which goes beyond SCF in an attempt to treat this observable fact properly, is known as an electron correlation method or a post-SCF method.

Configuration interaction

Configuration interaction (CI) methods begin by noting that the exact wavefunction cannot be expressed as a single determinant, as Hartree-Fock theory assumes. [Foresman and Frisch, 1996] CI proceeds by constructing other determinants by replacing one or more occupied orbitals within the Hartree-Fock determinant with a virtual orbital. [Foresman and Frisch, 1996] In a single substitution, a virtual orbital replaces an occupied orbital within the determinant. This is equivalent to exciting an electron to a higher energy orbital. In the same manner, in a double substitution, $\phi_a \leftarrow \phi_i$ and $\phi_b \leftarrow \phi_j$, two occupied orbitals are replaced by virtual orbitals, for example:

$$\Psi_{ia} = |\phi_1, \ldots \phi_i, \phi_{a+1}, \ldots \phi_{i-1}, \phi_a, \ldots \phi_n| \qquad (4.13)$$

Similarly, triple substitutions would exchange three orbitals, and so on. The full CI method forms the wavefunction ψ as a linear combination of the Hartree-Fock determinant and all possible substituted determinants;

$$\psi = c_o\psi_{HF} + c_1\psi_1 + c_2\psi_2 + \ldots \qquad (4.14)$$

where the coefficients c reflect the weight of each determinant in the expansion and also ensures normalization.

Although the full CI method is well defined, size-consistent, and variational it is also very expensive and impractical for all but very small systems. Practical CI methods augment the Hartree-Fock by adding only a limited set of substitutions. Such methods will truncate the CI expansion at some level of substitution, for example, the CIS method adds single excitations to the Hartree-Fock determinant, CID adds double excitations, CISD adds singles and doubles, CISDT adds singles, doubles, and triples, and so on. [Foresman and Frisch, 1996]

One way to think about the Hartree-Fock process is that it is an optimization of orbitals subject to the constraint that single excitations do not contribute to the wavefunction. [Cramer, 2002] The CI-singles (CIS) method, on the other hand, can be useful for excited states. Some other methods used in the analysis of excited states are the complete active space multiconfigurational self-consistent field (CASSCF) method and the time-dependent Hartree-Fock or DFT method. Since only singlet excitations were of interest in the analysis of the near UV absorption spectrum of glyoxal, this was the method of choice.

Gaussian

The tool used to perform the computational calculations for this thesis Gaussian. Gaussian is a system of programs for performing a variety of semi-empirical and ab initio molecular orbital (MO) calculations. [Friedman and Frisch, 1999] The version of Gaussian used is the Gaussian 98 software. Gaussian 98 is capable of predicting many properties of molecules and reactions, including: 1) molecular energies and structures, 2) energies and structures of transition states, 3) vibrational frequencies, 4) IR and Raman spectra, 5) thermochemical properties, 6) bond and reaction energies, 7) reaction pathways, 8) molecular orbitals, 9) atomic charges, 10) multiple moments, 11) NMR sheilding and magnetic susceptibilities, 12) vibrational circular dichronism intensities, 13) electron affinities and ionization potentials, 14) polarizabilities and hyperpolarizabilities, and 15) electrostatic potentials and electron densities. [Freidman and Frisch, 1999] Gaussian 98 was instrumental in the course of this research to help model a portion of the continuous spectrum of glyoxal in the near-UV region, that is, 200-350 nm.

Gaussian input

Gaussian is known as a user-friendly program. It is

Table 4.1

Outline of Gaussian Input

Input Section	Contents
Link 0 Commands	Defines the locations of scratch files and job resource limits
*Route Section	Specifies the job type and model chemistry
*blank line	Separates the route section from the title section
*Title Section	Describes the job for the output and archive entry
*blank line	
*Molecule Specification	Gives the structure of the molecule to be studied
*blank line	
Variables Section	Specifies values for the variables used in the molecule specification
blank line	

also flexible and allows the usage of a variety of different tasks to be performed without the necessity of making changes to the overall structure of the program.

Gaussian input has the basic structure outlined in Table 4.1. Note that the input sections marked with an asterisk are required in every input file. [Friedman and Frisch, 1996]

Gaussian accepts molecule specifications in several different formats, for example, Cartesian coordinates and Z-matrix format (internal coordinates). Appendix B has a

detailed explanation of the Gaussian input file sections including, as an example an interpretation of one of the jobs performed for the purposes of this research.

Chapter V

Before reporting the results from the molecular calculations performed a brief discussion is dedicated to group theory. Also reported is the determination of trans-glyoxal's representations of its fundamental vibrational frequencies by applying group theory.

Group Theory

Symmetry and group theory can be powerful tools for studying bonding and spectroscopy. In fact, properties such as measurement of crystal structures, infrared spectra, ultra-violet spectra, dipole moments, and optical activities depend on molecular symmetry.

The basis for our understanding of molecular structure (rather than simply its determination) lies in quantum mechanics and, therefore, any consideration of the role of symmetry in chemistry is basically a consideration of its role in quantum mechanics. [Bishop, 1973] The link between symmetry and quantum mechanics is provided by that part of mathematics known as group theory.

For the purposes of molecular spectroscopy, it is routinely assumed that the internal energy of a system can be expressed as the sum of rotational, vibrational, and electronic contributions [Carter, 1998]:

$$E_{int} = E_r + E_v + E_e \qquad (5.1)$$

This implies the overall wavefunction is:

$$\Psi = \psi_r\psi_v\psi_e \qquad (5.2)$$

for which the individual energies are given by separate Schrodinger equations of the form $H\Psi=E\Psi$. Solution to these equations is greatly simplified by changing the coordinates of the nuclei from Cartesian coordinates to a new type, defined in a special way, called the normal coordinates.

In group theory, each normal coordinate belongs to one of the irreducible representations of the point group of the molecule concerned and it is a part of a basis, which can be used to produce that representation. The vibrational wavefunctions associated with the fundamental vibrational energy levels behave in the same way because of their relationship with the normal coordinates. [Bishop, 1973] It is, therefore, possible to classify both the normal coordinates and fundamental vibrational wavefunctions according to their symmetry species and to predict from the character tables the degeneracies and symmetry types which can, in principle, exist. [Bishop, 1973] Moreover, knowledge of the irreducible

representations to predict from the vibrational wavefunctions reveals a good deal about the spectra of the molecule under consideration.

Molecular vibrations

The mass weighted displacements of the nuclei of a molecule from their equilibrium position, q_I, can be used to generate a representation of the point group to which the molecule belongs. [Bishop, 1973] Under the symmetry operation, R, the mass weighted nuclear displacements q_1, q_2,…q_{3N} become q_1',q_2',…q_{3N}' then;

$$q_i' = \sum D_{ij}^{\circ}(R) q_j \qquad (5.3)$$

where i = 1,2,…3N. The matrices $D^{\circ}(R)$ contain 3X3 block matrices, one for each atom. For any operation R_i, all the individual-atom operator matrices (3X3 matrices) have identical form and therefore, have the same character, χ_i. [Carter, 1998] Only individual-atom block matrices that lie along the diagonal of the full operator matrix contribute to the overall operation, χ_R. Furthermore, only those 3X3 block matrices for the atoms that are not shifted by the operation contribute to the character of the overall matrix. Thus, to find χ_R, the number of atoms that remain

non-shifted by the operation are counted, N_i, and multiplied by the contribution per non-shifted atom, χ_I, that is;

$$\chi_R = N_i\chi_i \qquad (5.4)$$

where χ_i is equivalent to the character of the 3X3 block matrices of which the full matrix of the operation is composed. (Carter, 1998)

In an examination of the individual-atom transformation matrices comprising the full matrix for an operation, the individual elements c_{11},c_{22},c_{33} (along the trace of the 3X3 matrix) indicate the effects of the operation on the coordinates x,y,z, respectively, on the atoms on which they operate. Therefore, the values for these elements will be identical to the characters for the operation in the irreducible representations by which the unit vectors x,y,z transform. χ_i, then, is simply attained by adding up the characters in the character table under the operation for the irreducible representations by which all the three unit vectors transform.

Fundamental vibrational frequencies for glyoxal

Table 5.1 incorporates this instruction needed to generate the reducible representation for the fundamental vibrational frequencies of glyoxal in the C_2h trans-glyoxal

Table 5.1

Fundamental Frequencies for Trans-Glyoxal

C_2h	E	C_2	i	σ_h		
N_i	6	0	0	6		
χ_i	3	-1	-3	1		
Γ^{3N}	18	0	0	6	$\sum$	n_i
A_g	18	0	0	6	24	6
B_g	18	0	0	-6	12	3
A_u	18	0	0	-6	12	3
B_u	18	0	0	6	24	6

$$\Gamma^{3N} = 6A_g + 3B_g + 3A_u + 6B_u$$

configuration. It also notes the transformation properties of the unit vectors and rotational vectors from the character table. It shows that:

$$\Gamma_{3N} = 6A_g+3B_g+3A_u+6B_u \qquad (5.5)$$

There are, however, 3N-6=12 normal modes of vibration. The symmetry species of the genuine normal modes of vibration are identified by removing the species for the three translations and three rotations the molecule processes from Γ_{3N}, that is,

$$\Gamma_{3N-6} = \Gamma_{3N}-\Gamma_{trans}-\Gamma_{rot} \qquad (5.6)$$

For trans-glyoxal, $\Gamma_{trans} = A_u+2B_u$ and $\Gamma_{rot} = A_g+2B_g$. Applying Equation (5.6) gives;

$$\Gamma_{3N-6} = 5A_g+B_g+2A_u+4B_u \qquad (5.7)$$

corresponding to the normal vibrational modes for trans-glyoxal.

Allowed transitions

As mentioned previously, it is usually assumed that the internal energy of a molecule can be decomposed into rotational, vibrational and electronic components. The transition between an electronic ground state ψ_e and some excited state ψ_e' will be observable as a band in the absorption spectrum if there is a nonzero transition moment of the form:

$$M_e = \int\psi_e\mu\psi_e' \, d\tau \qquad (5.8)$$

in which μ is the electronic dipole moment operator whose components resolve as $\mu=\mu_x+\mu_y+\mu_z$.

Transitions that occur because the electronic wave functions are not fully independent of the vibrational

functions and the integral in Equation (5.9) can take on the form:

$$\int(\psi_e\psi_v)\mu(\psi_e'\psi_v')\ d\tau \qquad (5.9)$$

Because the vibrational ground state is totally symmetric, however, $\psi_e\psi_v$ has the same symmetry as ψ_e. ψ_v', on the other hand, may have the symmetry of any of the normal modes.

If any transition has the appropriate symmetry so that the direct product, $\psi_e\mu\psi_e'\psi_v'$, contains the totally symmetric representation then the integral will not vanish, that is it is allowed. [Carter, 1998] A similar analysis for trans-glyoxal, C_2h, illustrates that the transition $A_u \leftarrow A_g$ has the integral:

$$\Gamma^{Ag}\Gamma^{xyz}\Gamma^{Au} = A_g + 2B_g \qquad (5.10)$$

which contains the symmetric representation A_g. Thus, the transition $A_u \leftarrow A_g$ is allowed.

Chapter VI

As mentioned in Chapter I, the most characteristic electronic feature of the glyoxal molecule are the free oxygen non-bonding (n) orbitals and the π-orbitals on the C=O groups. Upon excitation of the glyoxal molecule, the $A_u \leftarrow A_g$ and $B_g \leftarrow B_u$ configurations are allowed whereas $B_g \leftarrow A_g$ and $A_u \leftarrow B_u$ are forbidden by symmetry.

Ab initio calculations can be useful for guiding the assignment of vibrational spectroscopy. Using the CIS method, the identification of the vibration observed in the continuous area of the glyoxal spectrum at the 280nm wavelength is described below.

Analysis of Gaussian calculations

Molecular systems have stable, higher energy electronic configurations known as excited states. Such states are produced, for example, when a sample is exposed to the light source of a UV/visible spectrophotometer. Modeling excited states and predicting their properties is a difficult problem; a theoretical method must avoid always ending up at the ground state. [Foresman and Frisch, 1996] The CI approach, named CI-Singles, models excited states as combinations of single substitutions out of the Hartree-Fock (HF) ground state. CI-Singles is described by its

developers as "an adequate zeroth-order treatment for many of the excited states of molecules," and in this sense is comparable to HF theory for ground state systems in that it is qualitatively accurate if not always highly quantitatively predictive. [Foresman and Frisch, 1996]

A more accurate method to study excited state system is the complete active space multiconfigurational self-consistent field (CASSCF). This method uses a combination of an SCF computation with a full configuration interaction calculation involving a subset of the orbitals.

The time-dependent (TD) method keyword in Gaussian can also be useful in excited state energy calculations using the Hartree-Fock or DFT method. In a TDDFT method, Kohn-Sham orbital energies and various exchange integrals are used in place of matrix elements of the Hamiltonian. [Cramer,2001] TDDFT results are most reliable when, i) the excitation energy is significantly smaller than the molecular ionization potential and ii) promotion(s) take place into orbitals having positive Kohn-Sham eigenvalues. [Cramer,2001]

The Gaussian 98 CIS feature affords the ability to optimize a geometry and perform frequency calculations for systems in an excited state. Using Gaussian 98, CIS, the first, second and third excited states of glyoxal were

located via an energy calculation. An optimization was then performed, starting from that point. Finally, frequencies were calculated at the optimized geometry. See Appendix B for a detailed explanation of the step job route section.

Job analysis

When requesting for the optimization of an excited state for glyoxal using the CIS method, the Gaussian output gives the energies, excitation and oscillator strengths of each computed excited state. For the second excited state analysis, the same input file as for the first excited state was used, only with the specified Root=2 in the route section. Root=3 was requested for the third excited state.

First excited state

The results for the frequency calculations of the DZP CIS level of theory for the first excited state of glyoxal are shown in Table (6.1). Listed are the vibrational frequencies and their corresponding motion. These motions were verified through a software package called Molden.

Molden

Molden can animate reaction paths as well as molecular vibrations from Gaussian run output files. It is a package for displaying molecular density from ab initio packages which includes the Gaussian 98 software. Molden reads all

Table 6.1

Results of the Frequency (cm^{-1}) Calculations for the First Excited State of Trans-Glyoxal Using the CIS Method

			Basis Set
		Trans isomer	6-31+G(D) ^1A_u state
υ_1	a_g	CH stretch	3187.6
υ_2	a_g	CO stretch	1876.5
υ_3	a_g	CH rock	1395.2
υ_4	a_g	CC stretch	1238.3
υ_5	a_g	CCO bend	626.4
υ_6	a_u	CH wag	805.4
υ_7	a_u	Torsion	263.0
υ_8	b_g	CH wag	905.4
υ_9	b_u	CH stretch	3179.8
υ_{10}	b_u	CO stretch	1846.8
υ_{11}	b_u	CH rock	1352.8
υ_{12}	b_u	CCO bend	259.1

the required information from the Gaussian output file. It can write a variety of graphics formats; (postscript, XWindows, VRML, povray, OpenGL, teckronics 4014, hpgl, hp 23929, and Figure).

The XWindows version of Molden is also capable of importing and displaying chemx, PDB, and a variety of mopac/ampac files and lots of other formats. [http://www.cmbi.kun.nl/~schaft/molden/molden.html] The Z-matrix format was the format used in the computational analysis of, this thesis.

Evaluation of CIS performance

Table 6.2 presents the 6-311++G(D,P) CIS frequency for trans- glyoxal in the A_u electronic state along with fundamental frequencies that have been observed directly in, or inferred from, experiments. The % error for each vibrational mode is also listed.

While it is certainly true that a comparison between calculated harmonic frequencies and measured fundamental vibrational transition energies is imperfect, harmonic correlations for excited electronic states should generally be similar to those in the ground states. That is, fundamental frequencies are less than 10% below the corresponding harmonic values for stretching modes and within a few percent (with uncertain sign) for bending and torsional vibrations. [Stanton and Gauss, 1997]

It can be seen from Table 6.2 that the agreement between the theoretical and experimental frequencies in both electronic states is acceptable. Table 6.3 reports the results obtain by Stanton and Gauss for the theoretical harmonic frequencies for the A_g and A_u electronic states for trans glyoxal using the EOMEE-CCSD level of theory.

The EOMEE-CCSD method is similar in spirit to single reference configuration using the same determinantal basis, but with a straightforward application of perturbation

Table 6.2

Results of the Frequency (cm^{-1}) Calculations for First Excited State of Trans-Glyoxal Using the 6-311++G(D,P) CIS Method

			Basis Set		
			6-311++G(D,P)	Experimental	%error
		Trans isomer	^1A_u state		
υ_1	a_g	CH stretch	3126.6	2809	11.3
υ_2	a_g	CO stretch	1859.3	1391	33.7
υ_3	a_g	CH rock	1384.8	1195	15.9
υ_4	a_g	CC stretch	1221.0	952	28.3
υ_5	a_g	CCO bend	624.9	509	22.8
υ_6	a_u	CH wag	797.7	720	10.8
υ_7	a_u	Torsion	261.7	233	12.3
υ_8	b_g	CH wag	899.6	735	18.5
υ_9	b_u	CH stretch	3118.8		
υ_{10}	b_u	CO stretch	1824.9	1281	42.5
υ_{11}	b_u	CH rock	1338.8	1172	14.2
υ_{12}	b_u	CCO bend	251.8	379	33.6

theory. [Stanton and Gauss, 1997] As noted in Table 6.3 EOMEE-CCSD is excellent for excited state descriptions, particular for those states that can be categorize as 'singly' excited states. The accuracy in performance can be attributed to its treatment of excited state electron correlation roughly comparable in quality to the corresponding ground state couple cluster method (CCSD) combined with computational scaling properties that allow its application to medium-sized molecules. [Stanton and Gauss, 1997] In comparison of Tables 6.2 and 6.3, it should be noted that a better agreement is attained using

Table 6.3

Results by Stanton and Gauss [1997] for the Frequency Calculations for the Ground and First Excited States of Trans-Glyoxal Using the EOMEE-CCSD Level of Theory

			Basis Sets			Basis Sets		
		Trans	6-31+G(D) ^1A_g state	6-311++G(D,P)	Exp.	6-31+G(D) ^1A_u state	6-311++G(D,P)	Exp.
υ_1	a_g	CH stretch	3057.2	3042.3	2843	3091.2	3070.9	2809
υ_2	a_g	CO stretch	1851.5	1821.6	1745	1582	1559.7	1391
υ_3	a_g	CH rock	1418.1	1413.2	1338	1277.5	1263.4	1195
υ_4	a_g	CC stretch	1117	1097.5	1065	1008.5	978.4	952
υ_5	a_g	CCO bend	567.3	562.8	551	515.1	513	509
υ_6	a_u	CH wag	837.3	821.8	801	768.3	758.8	720
υ_7	a_u	Torsion	145.7	126	127	239.4	232.9	233
υ_8	b_g	CH wag	1072.7	1081.3	1048	752.8	763.3	735
υ_9	b_u	CH stretch	3052.2	3035.9	2835	3091	3070.9	
υ_{10}	b_u	CO stretch	1809.7	1793.4	1732	1372.3	1402.9	1281
υ_{11}	b_u	CH rock	1372.5	1373	1312	1244.9	1250	1172
υ_{12}	b_u	CCO bend	338.1	340.8	339	390.9	397.7	379

the EOMEE-CCSD method.

In the implementation of the CIS method, the only significant difference between calculated and accepted values sum in Table 6.2 appears in the A_u state, where the carbonyl stretching frequencies V_2' and V_{10}' are overestimated by about 30% at the TZ2P CIS level of theory. Stanton and Gauss [1997] obtained agreement between 10-15%. It should be noted that the overestimation is qualitatively consistent with the finding that the experimentally

inferred internuclear separation is shorter than that predicted by calculation and thus, it appears that mode is relatively difficult to describe theoretically. [Stanton and Gauss, 1997]

Second excited state

For the second excited state, as stated earlier, he input file was the same as for the first excited state, except for the specified ROOT=2 in the route section. The results are given in Table 6.4.

In the output for the second excited state of trans-glyoxal, the transition $B_g \leftarrow A_g$ is observed. Inspection of the output reveals that the singlet B_g state has an oscillator strength of 0.0000, which means that it is a forbidden state and cannot be observed by single photon experiments, such as UV spectroscopy. [Foresman and Frisch, 1996] Any vibration, however, that distorts the molecule out of the C_2h symmetry will allow the molecule an excited state character.

It is known that geometry optimizations converge to a structure on the potential energy surface where the forces of the system reach equilibrium. Frequency calculations can be quite useful in disclosing the nature of a stationary point found by a geometry optimization. The final structure may correspond to a minimum on the

Table 6.4

Results of the Frequency (cm^{-1}) Calculations for the Second Excited State of Trans-Glyoxal Using the CIS Method

			Basis Sets	
			6-31+G(D)	6-311++G(D,P)
		Trans isomer		
υ_1	a_g	CH stretch	3214.2	3176.5
υ_2	a_g	CO stretch	1977.7	1812.9
υ_3	a_g	CH rock	1388.1	1325.6
υ_4	a_g	CC stretch	994.9	1016.4
υ_5	a_g	CCO bend	573.7	546.9
υ_6	a_u	CH wag	653.6	832.9
υ_7	a_u	Torsion	-155.6	354.4
υ_8	b_g	CH wag	812.3	850.4
υ_9	b_u	CH stretch	3206.6	3173.9
υ_{10}	b_u	CO stretch	1976.3	1702.3
υ_{11}	b_u	CH rock	1322.2	1301.1
υ_{12}	b_u	CCO bend	-98.2	438.8

potential energy surface, or it may represent a saddle point, which is a minimum with respect to some directions on the surface and a maximum in one or more others. [Foresman and Frisch, 1996] First order saddle points, which are a maximum in exactly one direction and a minimum in all other orthogonal directions, correspond to transition sate structures linking two minima. [Foreman and Frisch, 1996] In the output of a frequency calculation imaginary frequencies are indicated as negative numbers. A

structure which has n imaginary frequencies is an nth order saddle point. The frequency calculation of the optimized structure of the second excited state shows that the planar stationary point is not a minimum but has two imaginary vibrational frequencies. Whenever a structure yields an imaginary frequency, it means that there is some geometric distortion for which the energy of the system is lower than it is at the current structure (indicating a more stable structure).

First, for glyoxal the following processes are energetically possible at 308nm [Langford and Moore, 1984]:

$$(HCO)_2 + h\nu \rightarrow CO + CO + H_2 \qquad (6.1a)$$

$$\rightarrow H_2CO + CO \qquad (6.1b)$$

$$\rightarrow HCO + HCO \qquad (6.1c)$$

indicating that any of these dissociations could possibly be taking place.

Secondly, the transition $B_g \rightarrow A_g$, although forbidden, indicates that the transformation to the molecular orbital representation B_g facilitates any of the above dissociations. It should also be noted that the geometry optimizations of both the first and second excited states of trans-glyoxal show that the CC bonds are longer than in

the ground state. (The second excited state optimized CC bond is longer than the first excited state by approximately 0.1 angstrom).

Third excited state

The results of the third excited state can be seen in Table 6.5. It reveals that there is one imaginary vibrational frequency.

Table 6.5

Results of the Frequency (cm^{-1}) Calculations for the Third Excited State of Trans-Glyoxal Using the CIS Method

			Basis Sets	
			6-31+G(D)	6-311++G(D,P)
		Trans isomer		
υ_1	a_g	CH stretch	3218.8	3283.4
υ_2	a_g	CO stretch	1759.1	1968.5
υ_3	a_g	CH rock	1346.4	1356.9
υ_4	a_g	CC stretch	1211.1	1230.4
υ_5	a_g	CCO bend	392.8	394.2
υ_6	a_u	CH wag	618.6	620.0
υ_7	a_u	Torsion	-1746.7	-1713.2
υ_8	b_g	CH wag	695.4	704.0
υ_9	b_u	CH stretch	3189.4	3256.4
υ_{10}	b_u	CO stretch	1565.1	1583.0
υ_{11}	b_u	CH rock	1331.5	1347.7
υ_{12}	b_u	CCO bend	209.8	215.8

In 1981, Osamura et al., predicted constrained C_s stationary point geometries, possible transition states for the reaction:

$$(CHO)_2 \rightarrow H_2CO + CO \qquad (6.2)$$

Their results are given in Table 6.6. They performed the calculations with the split valence 3-21G basis set, configuration interaction was carried out including all configurations differing by one or two orbitals from the SCF reference configuration. [Osamura et al., 1981] Examining Table 6.6, it appears that for the trans-glyoxal, the 3-21G basis contains a single imaginary vibrational frequency which is sizable, i.e. 1739 cm^{-1} and does, indeed, connect glyoxal with formaldehyde plus carbon monoxide. The similar imaginary frequency of this study and that obtained in Table 6.5 suggests that the predicted third excited state for the 6-311++G(D,P) CIS level of theory leads to the dissociation in Equation 6.2.

Spectral Analysis

This section of the chapter incorporates the molecular calculations performed to the modeling of the glyoxal spectra experimentally obtained. The electronic absorption spectrum of a gas-phase molecule reveals electronic

Table 6.6

Results by Osamura et al. [1981] of the Vibrational Frequencies for the C_s Stationary Points Connecting Glyoxal with H_2CO + CO

		Basis Set
		3-21G
υ_1	a'	3200 cm^{-1}
υ_2	a'	2682
υ_3	a'	1984
υ_4	a'	1894
υ_5	a'	1308
υ_6	a''	1051
υ_7	a''	772
υ_8	a'	755
υ_9	a'	358
υ_{10}	a'	220
υ_{11}	a''	162
υ_{12}	a'	-1739

transitions consisting of a series of bands. Each band consists of a number of peaks. In the presence of a single progression, those peaks should have an approximately constant spacing in energy corresponding to a fundamental mode in the excited state. The range of the experimentally obtain spectra of glyoxal is from 200 to 350 nm. This near-UV region characterizes a continuous portion of the absorption spectrum. Table 6.7 reports each peak's the spacings are an average of 1470 cm^{-1}.

Table 6.7

Spacings for the Continuous Region of the Glyoxal Spectra at the 280 nm Wavelength

Wavelength (nm)	Wavenumbers (cm^{-1})	Spacing (cm^{-1})
255	39220	
264	37880	1340
275	36360	1520
287	34840	1520
298	33560	1280
311	32150	1410
328	30490	1660
346	28900	1590
	Average	1470

Based on the energies obtained from the computational results, the second excited state transition is in progress in the region of study. Examination of Table 6.3 indicates that the only fundamental vibrational frequency that corresponds to the spacing value of 1470 cm^{-1} is the A_g CO stretch. This, of course, is taking into account the overestimation characteristic of the CIS level of theory seen in the analysis of the first excited state.

The molecular orbital diagrams shown in Figure 1.4 (page 12) depict the fact that the transition to the excited electronic state molecular orbital representation

introduces a node between the carbon and oxygen bond for the $A_u \leftarrow A_g$ transition. This configuration, in essence, facilitates a CO stretch. In fact, the optimized structure of the excited state displays, as expected of the $\pi^* \leftarrow n$ type excitation process, the same effect; specifically, the CO bond length is increased due to a reduction in bond order while the CC bond distance contracts and the CCO angle opens slightly. (Stanton and Gauss, 1997) Thus, given the frequency calculations obtained computationally, using the CIS method, and the above factors, the assignment of the A_g CO stretch vibrational mode to the absorption peaks under study is evidently reasonable.

Chapter VII

Conclusion

In this thesis, comprehensive, medium resolution absorption cross-sections have been reported for the 280 nm gas-phase absorption spectra of glyoxal at room temperature. The results are in good agreement with at least one set of previously reported values.

The results of this study will be of use in the determination of glyoxal quantum yields and ultimately the rates and products of photolysis, as well as serve as input for laboratory studies of glyoxal chemistry where glyoxal concentration is determined by absorption spectroscopy. In addition, this cross-section data can be used to estimate the lifetime of glyoxal with respect to photodissociation for a representative set of tropospheric conditions.

Using the CIS method, molecular orbital calculations were also performed, as a guide to identify the vibration responsible for the weak structure features of the continuous region of the glyoxal spectrum centered at the 280 nm wavelength. The vibration accountable for the progression of peaks was found to be the A_g CO stretch vibration mode of the glyoxal molecule.

REFERENCES

Atkins, P.W. and R.S. Freidman, Molecular Quantum Mechanics, Oxford University Press, New York, 1997.

Atkinson, G.H. and C.S. Parmenter, The 260 nm Absorption Spectrum of Benzene: Remeasured Band Positions and Redefined Assignments, J. Mol. Spec., 73, 20-30,1978.

Bishop David M., Group Theory and Chemistry, Dover Publications Inc., New York, 1973.

Bretherick, L., Handbook of Reactive Chemical Hazards, Butterworths, London, 1985.

Calvert, J.C. and G. Lane, J. Am. Chem. Soc., 75, 856, 1953.

Carpenter, C.L. and L.S. Forester, The Spectra of Glyoxal Solutions, J. Phys. Chem., 62, 874-875, 1958.

Carter, R.L., Molecular Symmetry and Group Theory, John Wiley and Sons, Inc., New York, 1998.

Cramer, C.J., Essentials of Computatiuonal Chemistry: Theories and Models, Wiley, New York, 2002.

Drent, E. and J. Kommandeur, The Electronic States of Biacetyl, Chem. Phys. Letters, 14(3), 321-325, 1972.

Foresman, J.B. and A. Frisch, Exploring Chemistry with Electronic Structure Methods, Gaussian, Inc., Pittsburgh, PA, 1996.

Finlayson-Pitts, B.J. and J.N. Pitts, Jr., Chemistry of the Upper and Lower Atmosphere: Theory, Experiments and Applications, Academic Press, San Diego, CA, 2000.

Langford, A.O. and C.B. Moore, Collision complex formation in the reactions of formyl radicals with nitric oxide and oxygen, J. Chem. Phys., 80(9), 4211-4220, 1984.

Lewis, R.J., Hazardous Chemicals Desk Reference, John Wiley and Sons, Inc., New York, 1997.

Lui, Xiaoyu, H.E. Jeffries and K.G. Sexton, Atmospheric Photochemical Degradation of 1,4-Unsaturated Dicarbonyls, Environ. Sci. Technol., 33, 4212-4220, 1999.

Osamura, Yoshihiro and H.F. Schafer III, A unimolecular reaction ABC → A+B+C involving three product molecules and a single transition state. Photodissociation of glyoxal: HCOHCO → H_2+CO+CO, J. Chem. Phys., 75(12), 5828-5836, 1981.

Plum, C.N., E. Sanhueza, R. Atkinson, W.P.L. Carter and J.N. Pitts, Jr., OH Radical Rate Constants and Photolysis Rates of α-Dicarbonyls, Environ. Sci. Technol., 17(8), 479-483, 1983.

Smith, D.F., T.E. Kleindienst and C.D. McIver, Primary Product Distributions from the Reaction of OH with *m*-, *p*-Xylene, 1,2,4- and 1,3,5-Trimethylbenzene, J. of Atmos. Chem., 34, 339-364, 1999.

Stanton, J.F and J Gauss, Theoretical study of electronically excited cis- and trans-glyoxal, Spectrochimica Acta Part A, 53, 1153-1162, 1997.

Volkamer, R., U. Platt and K. Wirtz, Primary and Secondary Glyoxal Formation from Aromatics: Experimental Evidence for the Bicycloalkyl-Radical Pathway from Benzene, Toluene and *p*-Xylene, J. Phys. Chem., 105, 7865-7874, 2001.

Zhu, Lei, D. Kellis and Chuan-Fan Ding, Photolysis of glyoxal at 193, 248, 308 and 351 nm, Chem. Physics Letters, 257, 487-491, 1996.

APPENDIX A

Summary of Data

The experimental absorption cross-section data for the near UV absorption spectra of glyoxal is summarized below. The data is presented in tabular form, listing the wavelength (in nm) and the absorption cross-section (in pm^2, where 1 $pm^2 = 10^{-20}$ cm^2).

350	0.01564
349.5	0.02538
349	0.05358
348.5	0.13615
348	0.24919
347.5	0.30048
347	0.28811
346.5	0.31363
346	0.3535
345.5	0.32572
345	0.28266
344.5	0.26619
344	0.23847
343.5	0.17926
343	0.14051
342.5	0.13472
342	0.14847
341.5	0.16896
341	0.17032
340.5	0.17725
340	0.21211
339.5	0.23288
339	0.23907
338.5	0.25427
338	0.2448
337.5	0.23178
337	0.22568
336.5	0.23339
336	0.26611
335.5	0.31397
335	0.39632
334.5	0.4873

334	0.56436
333.5	0.60405
333	0.60472
332.5	0.62374
332	0.68699
331.5	0.77423
331	0.93282
330.5	1.15408
330	1.32369
329.5	1.42842
329	1.49908
328.5	1.53919
328	1.52476
327.5	1.45158
327	1.37655
326.5	1.31513
326	1.25559
325.5	1.22333
325	1.24635
324.5	1.29301
324	1.32324
323.5	1.3428
323	1.37977
322.5	1.4146
322	1.4409
321.5	1.48229
321	1.49616
320.5	1.48473
320	1.48237
319.5	1.51076
319	1.5876
318.5	1.72888
318	1.91212
317.5	2.04319
317	2.11299
316.5	2.19335
316	2.2792
315.5	2.3847
315	2.56855
314.5	2.7446
314	2.8549
313.5	2.94952
313	3.01892
312.5	3.01534
312	2.96134
311.5	2.89435
311	2.81531
310.5	2.75617

310	2.74471
309.5	2.7495
309	2.75593
308.5	2.77542
308	2.80049
307.5	2.81729
307	2.83684
306.5	2.85835
306	2.85575
305.5	2.85689
305	2.88704
304.5	2.94105
304	3.01694
303.5	3.11971
303	3.23094
302.5	3.32468
302	3.41257
301.5	3.4954
301	3.54625
300.5	3.60104
300	3.67221
299.5	3.70997
299	3.72545
298.5	3.72408
298	3.68107
297.5	3.59999
297	3.51686
296.5	3.47282
296	3.45439
295.5	3.42996
295	3.39895
294.5	3.36069
294	3.31263
293.5	3.28709
293	3.2783
292.5	3.26437
292	3.2633
291.5	3.25929
291	3.26482
290.5	3.29443
290	3.34162
289.5	3.38333
289	3.40547
288.5	3.41798
288	3.41674
287.5	3.40681
287	3.39913
286.5	3.3797

286	3.35101
285.5	3.29436
285	3.23676
284.5	3.18922
284	3.13912
283.5	3.07497
283	2.9985
282.5	2.94629
282	2.89384
281.5	2.83296
281	2.78805
280.5	2.75158
280	2.70438
279.5	2.68132
279	2.66519
278.5	2.64876
278	2.64347
277.5	2.64156
277	2.63833
276.5	2.61144
276	2.58096
275.5	2.56133
275	2.53793
274.5	2.48997
274	2.44821
273.5	2.40901
273	2.34464
272.5	2.28025
272	2.22802
271.5	2.17487
271	2.11577
270.5	2.06307
270	2.00456
269.5	1.95963
269	1.93067
268.5	1.90115
268	1.88113
267.5	1.86943
267	1.85995
266.5	1.84463
266	1.81855
265.5	1.79842
265	1.78592
264.5	1.75947
264	1.73
263.5	1.69573
263	1.65402
262.5	1.59957

262	1.54213
261.5	1.49279
261	1.44362
260.5	1.40386
260	1.37352
259.5	1.34606
259	1.31386
258.5	1.28633
258	1.27658
257.5	1.26723
257	1.25248
256.5	1.23726
256	1.21107
255.5	1.18538
255	1.16854
254.5	1.14516
254	1.10151
253.5	1.05602
253	1.01873
252.5	0.98378
252	0.94512
251.5	0.89631
251	0.86514
250.5	0.84465
250	0.8201
249.5	0.80348
249	0.79451
248.5	0.78128
248	0.76942
247.5	0.75185
247	0.7276
246.5	0.70249
246	0.67948
245.5	0.65572
245	0.62078
244.5	0.59214
244	0.55583
243.5	0.53424
243	0.51691
242.5	0.49446
242	0.47621
241.5	0.45457
241	0.44916
240.5	0.4385
240	0.42026
239.5	0.41432
239	0.39547
238.5	0.37234

238	0.36445
237.5	0.34772
237	0.31477
236.5	0.29247
236	0.28407
235.5	0.27268
235	0.26506
234.5	0.25609
234	0.24458
233.5	0.24723
233	0.24774
232.5	0.23511
232	0.2254
231.5	0.21625
231	0.21167
230.5	0.21
230	0.20344
229.5	0.19975
229	0.20141
228.5	0.20371
228	0.19764
227.5	0.20029
227	0.21675
226.5	0.22675
226	0.23043
225.5	0.2329
225	0.24098
224.5	0.25236
224	0.25592
223.5	0.26039
223	0.27516
222.5	0.29298
222	0.32098
221.5	0.35228
221	0.36482
220.5	0.38255
220	0.42322
219.5	0.45755
219	0.48891
218.5	0.53558
218	0.58146
217.5	0.63537
217	0.68982
216.5	0.74847
216	0.83482
215.5	0.93021
215	1.02616
214.5	1.13169

214	1.24571
213.5	1.36316
213	1.5051
212.5	1.67057
212	1.87116
211.5	2.14087
211	2.46174
210.5	2.8669
210	3.35795
209.5	4.01682
209	4.57524
208.5	5.14656
208	5.5942
207.5	7.52821
207	8.00871
206.5	8.88536

APPENDIX B

Gaussian Input File Format

Using as an example of the computational jobs performed to illustrate a Gaussian 98, a copy of an input file is given and its basic structure is described below.

Job File Input

```
%chk=tst
# RCIS/6-31+G(D) Test

glyoxal excited states

0 1
c
c 1 1.0
o 1 1.22 2 120.0
h 2 1.0  1 120.0 3 0.0
h 1 1.0  2 120.0 4 180.0
o 2 1.22 1 120.0 3 180.0

--Link1--
%chk=tst
%NoSave
#    RCIS(Root=1,Read)/6-31+G(D) Opt F r e q  Geom=Check
Guess=Read Test

frequencies

0 1
```

Route Section

Keyword (Option)	Description
%chk=tst	A check point file created by the program.
#RCIS	Requests a CI-singles excited state calculation, preceded by R for restricted calculations.

6-31+G(D), 6-311++G(D,P) Describes the type of basis set.

Test Commands Gaussian not to enter the results of the current job in the archive.

--Link1-- Starts a new job.

%NoSave Tells the program to delete the checkpoint file after the step concludes eventhough %chk has been included.

RCIS(Root=n) Specifies which excited state is to be studied.

RCIS(Read) Reads the initial guesses for the CI-Singles states from the checkpoint file. This option is used to perform an additional job step for an excited state computed during the previous job step. It is accompanied by Guess=Read and Geom=Check.

Opt Tells the program to optimize the molecule at the level of theory described.

Freq Requests a frequency calculation.

Title Section

The title section consists of one or more lines of descriptive information about the job. This section is terminated by a blank line.

Specifying Molecular Structure

This section specifies the molecular structure of the system. Gaussian 98 accepts molecule specifications in different formats: 1) Cartesian coordinates, 2) Z-matrix format (internal coordinates) and 3) mixed internal and Cartesian coordinates.

All the aforementioned formats require that the charge and the spin multiplicity of the system be specified first. "0" was used for the charge to represent a neutral trans-glyoxal molecule. The spin multiplicity is given by the equation 2S+1, where S represents the total spin for the system. Since the restricted CIS was used, all the electrons are paired and have no contribution for the S (the +1/2 and -1/2 cancel each other). Consequently, the system has a multiplicity of "1".

For the description of each atom in the molecule, the Z-matrix syntax was followed as the format of choice. It specifies the locations of, and bonds between atoms using bond lengths, bond angles, and dihedral (torsion) angles.

First, carbon 1 was selected as the starting atom in the molecule, making it the origin of the molecule in space. Secondly, another carbon atom (carbon 2) was connected to the first carbon atom, placing it along the z-axis and specifying the length of the bond. Third, oxygen

was chosen as the third atom bonded to carbon 1 by a distance of 2.0 and specifying the angel formed by the two bonds, that is, 120°.

Finally, the positions of all the subsequent atoms were specified by: 1) its atom label; 2) an atom to which it is bonded to and the bond length; 3) a third atom to it (or to the second atom) and the value of the resulting bond angle; 4) a fourth atom bonded to either end of the previous chain and the value of the dihedral (torsion) angle formed by the four atoms. Dihedral angles describe the angle the fourth atom makes with respect to the plane defined by the first three atoms; their values range from 0 to 360 degrees, or from -180 to 180 degrees.